ISTANBUL TECHNICAL UNIVERSITY ★ ENERGY INSTITUTE

COMPARISON OF BETA, NEUTRON AND GAMMA ATTENUATION PROPERTIES OF PMMA/COLEMANITE COMPOSITES

M.Sc. THESIS

Shima MEHRANPOUR

Nuclear Researches Division

Radiation Science and Technology Programme

DECEMBER 2019

ISTANBUL TECHNICAL UNIVERSITY ★ ENERGY INSTITUTE

COMPARISON OF BETA, NEUTRON AND GAMMA ATTENUATION PROPERTIES OF PMMA/COLEMANITE COMPOSITES

M.Sc. THESIS

Shima MEHRANPOUR
(302161021)

Nuclear Researches Division

Radiation Science and Technology Programme

Thesis Advisor: Prof. Dr. Nilgün BAYDOĞAN

DECEMBER 2019

İSTANBUL TEKNİK ÜNİVERSİTESİ ★ ENERJİ ENSTİTÜSÜ

PMMA/KOLEMANİT KOMPOZİTLERİN BETA, NÖTRON VE GAMMA ZAYIFLATMA ÖZELLİKLERİNİN KARŞILAŞTIRILMASI

YÜKSEK LİSANS TEZİ

Shima MEHRANPOUR
(302161021)

Nükleer Araştırmalar Anabilim Dalı

Radyasyon Bilim ve Teknoloji Programı

Tez Danışmanı: Prof. Dr. Nilgün BAYDOĞAN

ARALIK 2019

Shima MEHRANPOUR, a M.Sc. student of ITU Institute of Energy student ID 302161021, successfully defended the thesis entitled COMPARISON OF BETA, NEUTRON AND GAMMA ATTENUATION PROPERTIES OF PMMA/COLEMANITE COMPOSITES", which she prepared after fulfilling the requirements specified in the associated legislations, before the jury whose signatures are below.

Thesis Advisor :	**Prof. Dr. Nilgün BAYDOĞAN** İstanbul Technical University	.....
Jury Members :	**Prof. Dr. Nesrin ALTINSOY** Istanbul Technical University	.....
	Dr. Ayhan AKKAŞ Turkish Atomic Energy Authority	.....

Date of Submission : 13 November 2019
Date of Defense : 13 December 2019

To my family,

FOREWORD

I would like to express my thankfulness to my advisor Prof. Dr. Nilgun Baydogan for her motivations, guidance and support during the preparation of this thesis.
I am also thankful to my laboratory colleagues for the support and encouragement.
I especially thank to Prof.Dr. Adnan Tekin Materials Science and Production Technologies Applied Research Center (ATARC) for the help and support during this master thesis.
I am deeply thankful to my family for their continuous support, encouragement and love.

December 2019

Shima MEHRANPOUR
(Nuclear Physicist)

TABLE OF CONTENTS

Page

ABBREVIATIONS

ATRP **:** Atom Transfer Radical Polymerization
Bu_4NBr **:** Tetra-n-butylammonium bromide
EBiB **:** Ethyl 2-bromoisobutyrate (EBiB)
MMA **:** Methyl Mehacrylate
PMDETA **:** 1, 1, 4, 7, 7- Pentamethyldiethylenetriamine
PMMA **:** Poly (methyl methacrylate)
PVC **:** Polyvinyl Chloride

LIST OF TABLES

Page

LIST OF FIGURES

Page

COMPARISON OF BETA, NEUTRON AND GAMMA ATTENUATION PROPERTIES OF PMMA/COLEMANITE COMPOSITES

SUMMARY

Poly (methyl methacrylate) (PMMA) is a thermoplastic material with high resistivity against abrasion and heat. PMMA material has great thermal, mechanical and radiation shielding properties which can be improved by the addition of colemanite filler. Based on superior structural properties of PMMA material and the addetives (colemanite filler), the produced PMMA based polymer composites can be used in different application areas such as the aviation and aerospace field. These new materials have significant advantages such as high durability and high strength.

PMMA is a transparent thermoplastic polymer material from the acrylate family. PMMA reinforced by colemanite filler has great importance in various applications ranging from large scales to small scales. Three main polymerization methods that can be used in the production of PMMA polymer composites are solution-mixing, melt-compounding and in-situ polymerization. The Atom Transfer Radical Polymerization (ATRP) method was used to disperse colemanite filler into PMMA material, in this study. Colemanite was used to enhance the radiation shielding properties of PMMA.

Beta, neutron and gamma transmission techniques were applied to investigate the behavior of PMMA/Colemanite composite samples against radiation. Cs-137 and Co-60 were used as gamma source, Sr-90 was utilized as beta source and Pu-Be neutron Howitzer (NH_3) was used in neutron transmission test.

PMMA/Colemanite composite samples were produced at three different concentrations of colemanite and irradiated for determined duration, then the linear attenuation coefficient values were calculated for Cs-137, Co-60 and Sr-90 radioisotopes and the total macroscopic cross-sections values were evaluated for neutron source with the rise of colemanite content in samples.

The results indicated that by the rise of colemanite concentration, the linear attenuation coefficients and the mass attenuation coefficients were increased slowly. Based on this fact, it is possible to improve the radiation shielding properties of PMMA based polymer by the addition of colemanite as a filler.

PMMA/KOLEMANİT KOMPOZİTLERİN BETA, NÖTRON VE GAMMA ZAYIFLATMA ÖZELLİKLERİNİN KARŞILAŞTIRILMASI

ÖZET

Poli (metil metakrilat) (PMMA), aşınma ve ısıya karşı yüksek direnci olan termoplastik bir malzemedir. PMMA malzemesi, kolemanit takviye malzemesinin eklenmesiyle geliştirilebilecek termal, mekanik ve radyasyondan koruyucu özelliklere sahiptir.

PMMA malzemeler, yüksek dayanıklılık ve yüksek mukavemet gibi önemli avantajlara sahiptir. PMMA'nın başlıca özelliklerini sıralamak gerekirse; uygun optik özelliklere sahip olması, saydamlık ve parlak görünüm sergilemesi, rijitliği, sertlik ve çizilmeye karşı dayanıklılığı şeklinde belirtmek mümkündür.

PMMA, akrilat ailesinden gelen şeffaf bir termoplastik polimer malzemedir. Güneş ışınlarına (ultraviyole radyasyonu) ve hava etkisiyle aşınmaya karşı dirençli malzemelerdir.

Kolemanit dolgusu ile güçlendirilmiş PMMA, büyük ölçeklerden küçük ölçeklere kadar çeşitli uygulamalarda büyük öneme sahiptir. PMMA polimer kompozitlerinin üretiminde kullanılabilecek üç ana polimerizasyon metodu çözelti karıştırma, eritmeli bileşik ve yerinde polimerizasyondur.

Bu çalışmada kullanılan PMMA/Kolemanit kompozit malzemeler, Atom Transfer Radikal Polimerizasyonu (ATRP) yöntemi kullanılarak, canlı polimerizasyon tekniği ile üretilmiştir. Kolemanit, PMMA'nın radyasyon koruma özelliklerini arttırmak için kullanılmıştır.

Atom Transfer Radikal Polimerizasyon (ATRP) yöntemi ile üretilmiş canlı Poly (methl methacrylate) (PMMA) matrisli yapılar, farklı sahalarda kullanılabilen yeni nesil malzemelerdir.

Bu tezde, hafif ve dayanıklı, polimer matrisli kompozit malzemelerin üretilmesi ve radyasyon geçirgenliği özelliklerinin incelenmesi hedeflenmiştir.

Bu tez kapsamında PMMA matrise eklenen kolemanitin, PMMA/Kolemanit kompozit yapının farklı radyasyon tiplerini zıhlama özelliklerine etkileri incelenmiştir. Böylece, radyasyonu zırhlama kapasitesine sahip, özgün niteliklerde, polimer kompozit zırh malzemesinin radyasyon geçirgenlik özellikleri detaylı olarak incelenmiştir. Sonuç olarak malzemenin radyasyon geçirgenliğinin, kolemanit artışına bağlı olarak değişimleri detaylı olarak incelenmiştir.

Bu tez çalışmasında, ATRP yöntemiyle üretilmesi sağlanmış, polimer kompozit örneklerin farklı sahalarda kullanımının belirlenmesi için polimer kompozit malzeme yapısında, iyonizan radyasyonun PMMA kompozit örnekler ve kolemanit ($CaB_3O_4(OH)_3.H_2O$) takviyeli PMMA/Kolemanitin 15, 30 ve 40 (at. %) olmak üzere, üç farklı miktarda kolemanit takviyesinin yapılması ile kompozit örneklerin radyasyon karşısındaki davranışı incelenmiştir. Böylece, yüksek oranda bor mineral takviyeli ve hiç bor mineral takviye edilmemiş polimer örneklerin davranışları mukayeseli olarak incelenmiştir.

PMMA / Kolemanit kompozit örneklerinin radyasyona karşı davranışını araştırmak için beta, nötron ve gama transmisyon teknikleri uygulanmıştır. Gama kaynağı olarak Cs-137 ve Co-60, nötron kaynağı olarak Pu-Be içeren Nötron Howitzer (NH3) kullanılmıştır.

Bu tez çalışmasında Sr-90 radyoizotopu kullanılarak, polimer kompozit yapıya elektrikçe negatif yüklü beta parçaçıklarının etkisinin detaylarına değinilmiştir. Bu proje kapsamında, yapıya kolemanit takviyesinin beta radyasyonu geçirgenliğine etkisi mukayeseli olarak incelenmiştir.

Beta radyasyonunun malzemenin özelliklerine etkisi detaylı olarak incelenmiştir. PMMA numunelerinin Sr-90 radyoizotopu karşısında davranışları incelenerek, kalınlığın artışıyla numunelerin bağıl şiddet değerlerinde meydana gelen değişiklikler belirlenmiştir.

PMMA/Kolemanit kompozit numunelerinin üç farklı kolemanit konsantrasyonunda üretilmesi sağlandıktan sonra, Cs-137, Co-60 ve Sr-90 radyoizotopları için lineer zayıflama katsayısı değerleri hesaplanmış ve toplam makroskopik tesir kesiti değerleri incelenmiştir. Örneklerde kolemanit miktarının artışı ile nötron geçirgenliğinin değişimi mukayeseli olarak incelenmiştir.

Sonuçlar, kolemanit konsantrasyonunun yükselmesiyle lineer ve kütle zayıflatma katsayılarının arttığını göstermiştir. PMMA bazlı polimerin radyasyondan koruma özelliklerini dolgu maddesi olarak kolemanit ilavesiyle geliştirmek mümkündür.

Polimer kompozitlerin yapısında; matris yapı ve bu yapıyı kuvvetlendirmek için, yapı içerisinde çeşitli partiküller kullanılabilmektedir. Bu şekilde, kompozit yapının, radyasyonu zırhlamasının mümkün olduğunca artırılmasının sağlanmasına çalışılmıştır.

Bu tez çalışmasında kullanılan PMMA malzemesinin ve katkı maddelerinin (örneğin kolemanit gibi takviyelerin yapıya eklenmesi ile) üstün yapısal özellikler taşıması nedeniyle havacılık gibi farklı uygulama alanlarında kullanıldığı bilinmektedir.

Polimer kompozit yapıda kullanılan kolemanit partiküllerin, iyonizan radyasyonun soğurulmasına katkı sağladığı tespit edilmiştir. Bu çalışma sonunda, yapıya takviye edilen farklı miktarlardaki kolemanit partiküllerin ve polimer matrisin radyasyon karşısındaki davranışları mukayeseli olarak değerlendirilmiştir. Radyasyon tiplerine bağlı olarak, kolemanit takviyesi ile radyasyonu zırhlama özellikleri mukayeseli olarak belirlenmiştir.

Polimer kompozit yapının gama radyasyonu geçirgenliğini mukayeseli olarak değerlendirmek amacıyla, deneyden elde edilen deneysel kütle zayıflatma katsayısı değerleri, WinXCOM programında hesaplanan teorik kütle zayıflatma katsayısı ile karşılaştırılmıştır. Elde edilen teorik ve deneysel kütle zayıflatma katsayılarının uyumlu olduğu tespit edilmiştir.

Farklı tiplerdeki iyonizan radyasyon kaynaklarından elde edilen beta, gama ve nötron radyasyonlarına karşı tüm numuneler için yarı tabaka kalınlığı (HVL) değerleri hesaplanmıştır. Yarı tabaka kalınlığı değerlerinin PMMA / Kolemanit örneklerinde kolemanit konsantrasyonunun artmasıyla azaldığı tespit edilmiştir. PMMA polimere kolemanit ilavesi, yapının radyasyon zayıflatma özelliğini arttırmıştır.

Elde edilen sonuçlar, farklı gama enerjilerine göre karşılaştırıldı. Ayrıca, beta ve nötron parçacıkları için listelenen yarı tabaka kalınlığı sonuçları ayrı ayrı karşılaştırıldı.

Bu karşılaştırma, hem partikül/radyasyon enerjisi hem de incelenen örneklerde kolemanit konsantrasyonu esas alınarak yapılmıştır.

Bu sonuçlar, ATRP yöntemiyle üretilen PMMA/Kolemanit kompozitinin havacılık ve havacılık endüstrisi gibi çeşitli uygulama alanlarında uygun bir malzeme olarak kullanılabileceğini işaret etmektedir.

1. INTRODUCTION

1.1 Polymers and Polymeric Materials

1.1.1 Basics of polymers

The word "Polymer" came from the Greek word “polys” which means many and “meros” means parts and it refers to a large molecule which is made up of repeating units with identical structure. Therefore, polymers have high molecular weight compounds. These reaping unites are called monomers which are made up of linking the same or different kinds of atoms or groups of atoms together by covalent bonds [1].

Polymers form through the connection of Monomers to each other in a process that is called “Polymerization”. Formation process of polymer occurs by linking monomer molecules together through chemical reactions. Polymerization can be occurred naturally or synthetically (step-growth polymerization, radical polymerization and ionic polymerization) [2].

Number of repeating unite “-mer” determines the degree of polymerization (DP). Based on the polymerization technique, the produced polymers show many different structures. Polymers have several structures such as; a) linear, b) branched, c) cross-linked, d) star, e) ladder and f) dendrimer structure, that each of which has different properties [3].

The properties of polymers can also be determined by different amounts of monomers and the intermolecular forces between them. Crystalline polymer structure can be formed when monomers lying parallel to each other. The non-parallel type of connections between monomers results in the formation of an amorphous region in the structure of polymer [4].

The advantages that make polymer an ideal material in many application areas are such as lightweight, low cost, high durability, easy processing, corrosion resistance, desired

design possibilities, low electrical and thermal conductivity, wide choice of colors, transparencies [5].

Due to their behavior against heat, polymers can be classified into two groups as thermosets and thermoplastics [6];

- Thermoplastics: Thermoplastics can become softened and melted when heated but they can be hardened again when cooled. These materials present no chemical or mechanical changes when they cooled and heated multiple times. Thus, these materials are recyclable even if they are used many times. They can show linear structure or branched chain. Polythene, polyester and PVC are some examples for this group of polymers [7].
- Thermosets: These cross-linked polymers are rigid and have high thermal stability. Thermosets are hard and resistant against heat. Some of the materials that carry thermosets characteristics are a) epoxy, b) resin, c) polyurethanes, d) bakelite, and e) vulcanized rubber [8].

The comparison of thermoplastic materials and thermoset materials, presented in Figure 1.1:

1. Thermosets are known to be resistant against high temperatures while thermoplastic materials can be melted when heated.
2. Thermoplastics are resistant to some organic solvents.
3. Thermoset polymers are so hard to be remolded or reshaped.
4. Thermoplastic materials can have transparency property due to their production method.
5. Thermosets have cross-linked structure while thermoplastics have straight chain.
6. Thermoplastics are highly recyclable but thermosets can't be recycled [6].

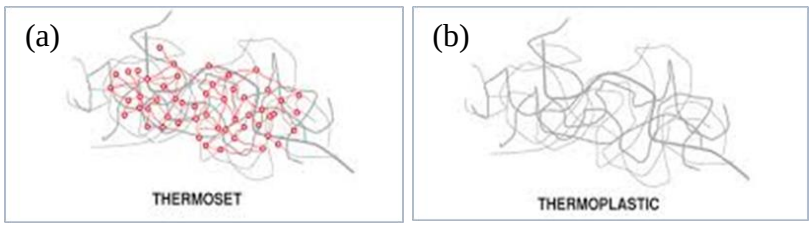

Figure 1.1 : a) Thermoset materials and b) Thermoplastic materials.

1.1.2 Main characteristics and application areas of PMMA

Poly (methyl methacrylate) or PMMA is a kind of acrylic thermoplastic polymer which has $(C_5H_8O_2)_n$ chemical formula. PMMA can be synthesized via radical polymerization technique by using methyl methacrylate (MMA) as monomer.

PMMA has repeating units. Chemical structure of PMMA is presented in Figure 1.2.

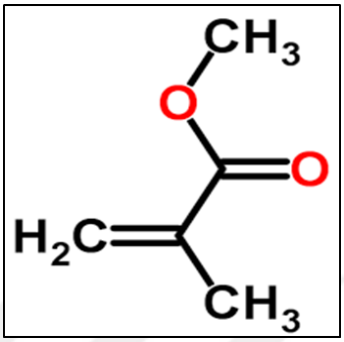

Figure 1.2 : Poly (methyl methacrylate).

Radical polymerization technique used for polymerization of PMMA using MMA is given in Figure 1.3.

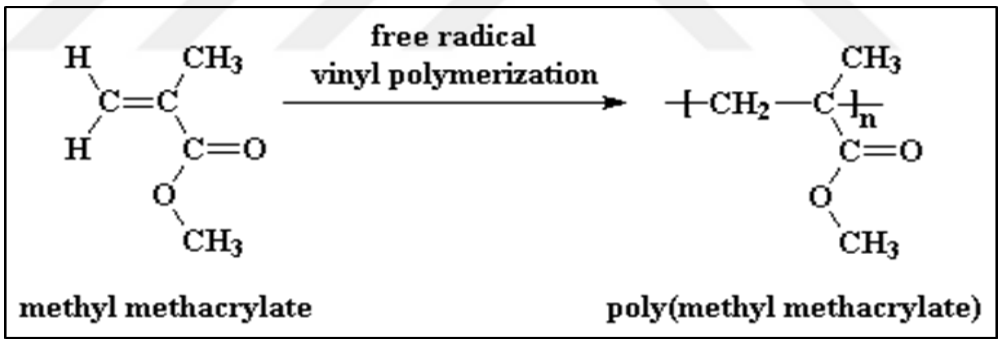

Figure 1.3 : Synthesis of PMMA via radical polymerization.

1.1.2.1 Characteristics of PMMA

The main characteristics that make PMMA applicable in large areas can be explained as below:

1. Physical properties: PMMA is a clear, colorless polymer and its density at room temperature is about 1.18-1.20 g/cm3 that is less than the density of glass. It is resistant to hardness and scratching. PMMA takes place in thermoplastic group of polymers and belongs to the acrylates. It has water absorptivity of 0.3-2% at room temperature [9-11].

Main physical characteristics of PMMA are listed below (Table 1.1).

Table 1.1: Main physical characteristics of PMMA.

Properties	Value
Density	1.18-1.20 g/cm3
Water Absorption	0.3 – 2 %
Transmission, Visible	~ 92 %
Refractive Index	~ 1.49
Hardness, Rockwell M	63 - 97
Young's modulus	1.8-3.2 GPa
Tensile Strength	47 - 79 MPa
Compression strength	70-120 MPa
Electrical Resistivity	~ 10_{15} Ω.cm
Thermal Conductivity	~ 0.2 W/m.K
Glass Temperature	~ 105 °C
Softening Point	~ 115°C
Melting Point	~ 160 °C

2. Optical properties: PMMA transmits up to 92% of visible light. The harmful ultraviolet light can be filtered and absorbed by PMMA material. Here, the C=O group is the absorber of UV radiation [9-11].

3. Thermal properties: Standard PMMA has thermal stability of 65˚C. Maximum withstanding temperature for the heat resistance performance of PMMA is around 100°C, and the minimum withstanding temperatures for it, is around −60°C. PMMA has relatively low specific heat in comparison to the rest of thermoplastic materials. It has high resistivity at low temperatures and has capability of tolerating temperatures of about -70 ˚C [9-11].

Important thermal characteristics of PMMA listed below (Table 1.2):

Table 1.2: Thermal characteristics of PMMA.

Properties	Value
CTE, linear 20 °C	60-130 µm/m. °C
CTE, linear 20 °C Transverse to Flow	70-90 µm/m. °C
Specific Heat Capacity	1.46-1.47 J/g. °C
Thermal Conductivity	0.19-0.24 W/M.K
Maximum Service Temperature, Air	41-103 °C
Melting Point	130 °C
Softening Point	47-117 °C
Glass Temperature	100-105

4. Mechanical characteristics: PMMA can be counted as one of the hardest materials in thermoplastics family. It is resistant against scratch and has a great mechanical strength property. PMM does not break or shatter when ruptured. Its capacity for absorbing moisture and water is so low. Thus, the products of PMMA present suitable dimensional stability property. The explained characteristics increase by the rise of temperature. Its mechanical performance does not show any significant changes between −60 °C and +70 °C. But PMMA is a breakable polymer material [9-11].

Mechanical characteristics of PMMA materials are listed below (Table 1.3):

Table 1.3: Mechanical characteristics of PMMA.

Properties	Value
Hardness, Rockwell M	63-97
Tensile Strength	47-79 MPa
Elongation at Break	1-30 %
Tensile Modulus	2.2-3.8 GPa
Flexural Modulus	3-3.5 GPa
Izod Impact, Notched	1.2-20 kJ/m^2
Izod Impact, Unnotched	11kJ/m^2
Tensile Creep Modulus, 1h	1800-2700 MPa
Tensile Creep Modulus, 1000h	1200-1800

5. Electrical characteristics: PMMA has low capacity of absorbing water and shows relatively high dielectric characteristics. Relative humidity of air, temperature, weather and frequency effects dielectric constant [9-11].

Electrical characteristics for PMMA are given below (Table 1.4):

Table 1.4: Electrical characteristics of PMMA.

Properties	Value
Electrical Resistivity	10^{14}-10^{15}Ω.cm
Surface Resistance	10^{14}-10^{16} Ω
Loss factor, 20 °C, 1000 Hz, 60% humidity	0.04
Dielectric Constant	2.8-4
Dielectric Constant, Low Frequency	3-4
Dielectric Strength	17.7-60 kV/mm
Dissipation Factor	0.03-0.55
Arc Resistance	100-180

6. Chemical properties: PMMA can be affected by Organic solvents and it becomes durable against many chemicals. PMMA is resistant to some chemical substances such as acid, alkaline, non-oxidizing acids, salts, but not resistant

to some other materials such as acetone, methylene chloride, chloroform, toluene, carbon tetrachloride, benzene, ethyl ether, xylene, butanone, methanol and acid oxidation in concentrated form. Hardenability of PMMA resembles copper hardness.

7. Combustibility: PMMA is a combustible material [10].
8. Hydrolysis resistance: In comparison to other polymer materials, PMMA has very high hydrolysis resistance.
9. Weathering resistance: In small quantities, PMMA can be affected by the change in transparency and color. PMMA has high weathering resistance among other polymer materials.
10. Resistant against radiation: PMMA shows a relatively high resistivity against ionizing radiation that is capable of damaging materials [41].

1.1.2.2 Application areas of PMMA

Optics, Vehicles, Office equipment, Medicine and Electronic devices are some industrial fields in which PMMA has significant importance. Main application areas of PMMA are explained below:

1. Signs and Displays
2. Construction and Architecture
3. Automotive and Transportation
4. Lighting
5. Electronics
6. Medical and Health
7. Furniture and Design [12]

1.2 Colemanite and Colemanite-Derived Materials

The mineral colemanite is one of the stable borate minerals, forms together with other borates in evaporite deposits of alkaline lacustrine sediments. Boron exists as an oxygenated compound of element boron in nature, primarily found in minerals as alkaline earth salts (alkali metal). Therefore, the chemistry of boron is based on B–O

compounds. Chemical reactions of borates are commonly characterized not by boron atom directly but with the interaction together with the associated oxygen atoms.

Colemanite is pyroelectric and Its chemical formula is (Hydrous calcium borate) $Ca_2B_6O_{11}\cdot 5H_2O$. During temperature changes, it produces an electrical charge and may develop dust on certain crystal faces due to a pyroelectric charge. Significant Features of colemanite are its crystal shape, hardness, cleavage, and occurrences [13].

Colemanite structure in Figure 1.4, shows the endless chains of interlocking $BO_2(OH)$ triangles and $BO_3(OH)$ tetrahedrons with calcium, water and extra hydroxide units which are interspersed between the chains [14].

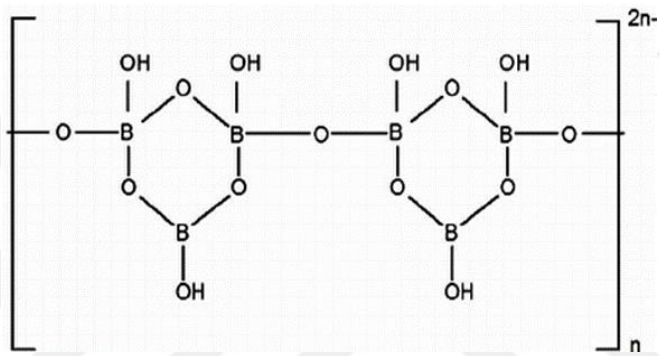

Figure 1.4 : Chemical structure of colemanite.

Colemanite increases the elastic modulus and the breaking strain while it decreases the yield stress and the yield strain of material. The added colemanite to polymer matrix can cause a reduction in its thermal expansion coefficient, due to lower thermal expansion coefficient of colemanite, respect to polymer matrix [15].

It is detected that increasing colemanite content enhances the stiffness of composite and the addition of colemanite can cause a noticeable rise in the fracture toughness characteristic of sample material. Thus, introducing a mineral filler to polymeric materials affects their toughness [16].

Main properties of colemanite can be classified as mechanical, physical, thermal, Optical and Electrical properties.

The developed crystals of colemanite are up to 2 or 3 inch in length. They are colorless and transparent, and the brilliant luster of their faces is vitreous to adamantine in character. A cleavage can be observed parallel to the symmetry of the crystals. The hardness of 4-4½ and specific gravity of 2.42 are recorded for this mineral [17].

For the production of basic chemicals, colemanite must be upgraded to an acceptable quality by mineral processing techniques. Boron minerals show a spectrum of solubilities dependent on the cations in the lattice structure and this spectrum of chemical compositions has a range of cations from monovalent to multivalent ions.

The solubility of the mineral can be determined by the type and valency of the cation and in turn controls its electro-kinetic behavior [18].

A drop appears in melting temperature of the mix by the addition of colemanite and it leads to low viscosity at the melting temperature, prevents crystallization and improves the chemical and physical characteristics of product. Colemanite reduces the melting point in glass industry and it is resistant to thermal shocks. Some of its advantages in formulation of ceramic and enamel glazes are such as; providing a stable structure, homogeneous melting and low segregation. It is a solvent for most of the metal oxides and can be utilized as a fluxing agent in metallurgy industry [19,20].

When boron minerals are heated, the mineral loses water of crystallization, followed by production of amorphous material or recrystallization into new phases. The decomposition process of colemanite mineral exhibits intra-crystalline thermal dissociation. While formation of the water molecules from OH groups in the structure takes place, water molecules which have been formed by this step, released by the heating energy. Two stages of this dissociation events are proceeded uniformly within the crystal grains of the mineral. Colemanite contains enclosed water molecules in the structure. The pressure from these enclosed H_2O molecules grows rapidly and leads to an explosive water loss with rising temperature. This sudden release in micropores results in the disruption of framework by the increase in temperature [21,22].

Therefore, utilizing the colemanite mineral as a raw material is limited in ceramic industry. On the other hand, deformation problems can appear in products when boron containing minerals of high amounts are used in ceramic products while they are densified in a fast firing process. based on this fact, to avoid such problems, colemanite mineral should be calcined before application for sintering aid [23].

1.3 Polymer Composites

A composite is a combination of a polymer matrix material with fillers and it is known as a new material with superior properties.

Enhancing the poor characteristics of polymer matrix materials, such as; thermal performance, mechanical properties and conductivity along with keeping the supreme properties of them at the same time, became possible by introducing polymer composite materials.

The interaction of polymer and fillers in polymer composites introduces a new material with great characteristics. Composite materials can be classified based on the type of matrix material, type of reinforcing fibers or fillers and form of dispersed phase.

Polymer composites make it possible to reinforce the polymer properties with fillers. The property improvements can be obtained with well-dispersed fillers in the host polymer matrix at low filler concentration. The decrease in the interparticle distance and increase in polymer matrix interaction strength occur by the addition of fillers with high surface energy, high surface area and anisotropic geometry in the polymer matrix.

Polymer matrices such as; thermoplastic resins, thermoset resins, and elastomers are explained below:

1. Thermoplastic resins that has a structure made up of long chains. It can be softened When heated. Some examples of this group are; PVC, PC, PMMA.
2. Thermoset resins with crosslinked chains are composed of resins. This group is heat resistant. Epoxy and amino are the examples for this group.
3. Elastomers: Natural and synthetic rubber can be classified as the examples of this group. Fillers are changeable for different applications.

Since it is possible to improve the weak characteristics of the polymer matrix by adding fillers to obtain materials with excellent properties and reasonable production costs Thus, polymer composites are more preferable than conventional composites [24].

Some advantages of polymer composite materials are their high stiffness, lightweight, great corrosion and abrasion resistance and high strength. These advantages can be explained based on the fact that fillers enhance the thermal, mechanical and optical characteristics of polymer matrix material to a great extent.

In different application areas, polymer composites improve the properties of host polymer in an incomparable way than conventional composites, due to the outstanding advantages mentioned above [25].

1.4 Purpose of This Study

Polymer composites are applicable in different areas such as aerospace, electronics, construction, biomedicine, solar cells, etc. The great features of additive fillers can be used to improve the poor properties of the host material.

In this research, PMMA is used for polymer matrix and the radiation attenuation property of polymers are evaluated as a function of colemanite concentration in samples.

The aim of this study is to gain deep insight about the preparation and characterization of polymer composites along with researching about the influence of the used filler on polymer matrices such as interactions with the polymer matrix and the corresponding improvements in properties of PMMA.

2. BACKGROUND

2.1 Process of Synthesizing PMMA Using ATRP

The polymerization methods to synthesize PMMA using methyl methacrylate (MMA) are a) free radical polymerization, b) emulsion polymerization, c) solution polymerization, d) anionic polymerization, and e) bulk polymerization.

ATRP (Atom Transfer Radical Polymerization) is the most commonly utilized technique for a controlled radical polymerization that can polymerize the monomer (MMA) to obtain PMMA material that can be defined as living polymer with great quality. ATRP is an effective method with controlled functionalities, topologies and compositions that provides producing well-defined polymers easily [26].

2.2 ATRP Components

Synthesize of PMMA via ATRP has six main components, shown with structure below (Figure 2.1) [35]:

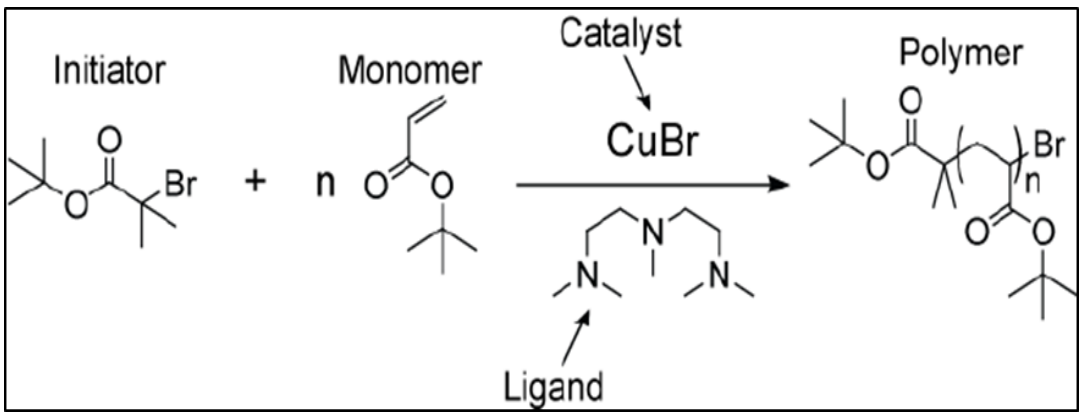

Figure 2.1 : Components of ATRP.

Fundamental components of ATRP method are monomer, initiator, catalyst, ligand, solvent and temperature. In this study:

1. Monomer is MMA or Methyl methacrylate.

2. Initiators are Alkyl halides R-X (X=Cl, Br) in this method. These initiators contain one or more atoms of halogen.
3. Catalyst is a transition metal species (M_{tn}) that has two available oxidation states and generally used for lowering or increasing these states.
4. Solvent increases the solubility of catalysts complex which directly influences the rate of reaction in polymerization process and the atom transfer equilibrium.
5. Ligand is a metal complex. A covalent or an ionic bond connects it to the catalyst. Solubilizing of the metal ion becomes possible by ligand. The choice of an appropriate ligand for reaction is very essential because it has great impact on the controlled polymerization.
6. Temperature is one of the important factors that has a direct effect on the rate of polymerization.

2.2.1 Methyl methacrylate (MMA)

In ATRP method, MMA is the monomer for the PMMA polymerization. MMA is a colorless liquid monomer and its chemical formula is $C_5H_8O_2$. The chemical bonds and structure of MMA is shown below (Figure 2.2):

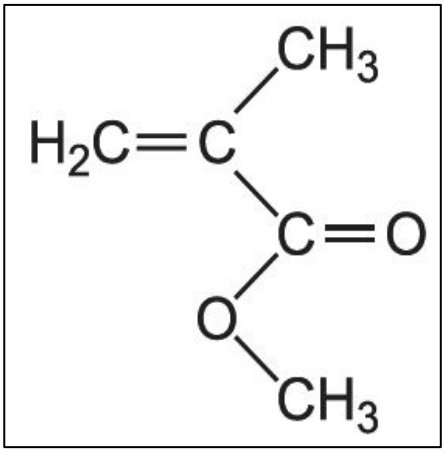

Figure 2.2 : Methyl methacrylate (MMA).

MMA has the largest ATRP equilibrium constant ($K_{eq}=k_{act}/k_{deact}$) in comparison to the other monomers. Some of its advantages are; a) abrasive resistance, b) great durability, c) transparency and d) strength.

Main characteristics of Methyl methacrylate (MMA**)** are listed in Table 2.1.

Table 2.1: Main characteristics of Methyl methacrylate.

Properties	Value
Density	0.94 g/cm3
Molar mass	100.12 g/mole
Boiling point	100.6°C
Melting point	-48°C
Flashpoint	8°C
Polymerization heat	53.97 kJ/mole

2.2.2 Initiator

Alkyl halides (RX) are widely used as the initiator in the polymerization process of MMA using ATRP technique. The rate of polymerization process can be determined from the concentration of Alkyl halides [27].

The characteristics of halide groups are important to obtain polymers with great qualities. Thus, an essential part of the final material is the complete initiator molecule. The obtained PMMA has high quality when halide group X is bromine or chlorine. Some examples of good initiators are; a) CCl_3COCH_3, b) $CHCl_2COPh$, c) dimethyl 2-bromo-2 and d) 4-trimethylglutarates. Some of initiators are very active that can cause an excessive termination or some other side reactions. RX group is either a monofunctional or a multifunctional initiator. An important factor to provide a site for chain growth is the number of functional groups [27,28].

2.2.3 Catalyat

Catalysts are the necessary components in ATRP method that plays an essential role of determining the position of the atom transfer equilibrium. Both of the activating and deactivating components of catalytic system must be present at the same time.

The prerequisites for catalyst to get efficient transition are;

1. The catalyst should have at least two available oxidation states that are separated by a single electron.
2. There must be suitable position and dynamics for ATRP equilibrium in the particular system.
3. The catalyst must have a sensible affinity to a halogen.

4. There is a necessity for an expandable coordination sphere around the catalyst in the case of oxidation.

There is a large number of transition materials available for ATRP, because of the easy polymerization of MMA. Some examples of these transition materials are such as ruthenium, copper, nickel, iron, rhodium and palladium. The most widely used among them is copper based transition metal catalyst [28].

2.2.4 Ligand

In the ATRP method, ligand is another significant component for the conjunction with various transition metals and has a great effect on the controlled polymerization. Ligands play the essential role in solubilizing the transition metal salt into the organic media and adjusting the catalyst potential for appropriate reactivity.

Some of ligands that are widely in use for ATRP method are nitrogen and phosphorous-based ligands [27,28]. Examples of nitrogen-based ligands can be seen in Figure 2.3.

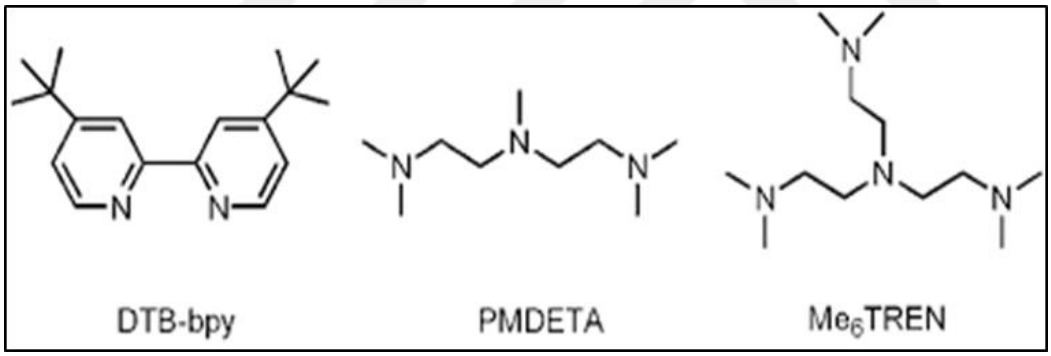

Figure 2.3 : Examples for ligand (nitrogen-based).

Three main advantages of ligands for an efficient polymerization are explained below:

1. Ligands control reaction via structural and electronic effects selectively.
2. In the reaction, ligands can solubilize the metal.
3. Ligands have influence on the oxidation-reduction chemistry of final metal complex.

The choice of ligand is an important factor in controlling the reaction and molecular weight in the system. Ligand adjusts the solubility of the catalyst to control the concentration of the activator and deactivator in reaction phase.

It enables the coordination sphere to expand and provides selective atom transfer without promoting any other reactions [29].

2.2.5 Solvent

The structure of a catalyst Complex can change by a variety of solvents. The atom transfer equilibrium and rate of polymerization process are affected by this change. Thus, the effect of solvent on ATRP method is so important. The choice of solvent is so essential to achieve an effective polymerization. Various solvents are in use for different monomers such as; alcohol, ethylene carbonate, ethyl acetate, toluene and benzene. The solvents that are used to improve the solubility of the catalyst complex are polar solvents. Using solvents become necessary when the formed polymers are not soluble in their monomers [27,28].

2.2.6 Temperature

Temperature plays an undeniable role in the polymerization process. High temperature increases the amount of heat loss and decreases the time for the completion of reaction. Due to the increase of collision frequency, a rise appears in the rate of reaction in high temperature. Temperature has direct effect on the polymerization rate. With the rise of temperature, the increase in both of the atom transfer equilibrium and the radical propagation rate constants leads to the increase in polymerization rate. Solubility of the catalyst decomposition happens by the rise of temperature.

Most of the MMA polymerizations performed in solution are at temperatures of about 70 to 90 °C. At high temperatures, the solubility of the catalyst increases. Also, chain transfer and other side reactions are remarkable at high temperature. Optimal temperature is dependent on catalyst, monomer and targeted molecular weight [27,28].

2.3 ATRP Mechanism

ATRP is a complex polymerization technique consist of three elementary reactions as below;

a) initiation.

b) propagation.

c) termination.

By controlling all of these three reactions and the reactivities of the involved species, suitable results for polymerization can be obtained [28].

1. Initiation: Initiator is the Thermal unstable part of this mechanism. It requires energy to split into two free radicals that contain unpaired electrons. The important factors that affect the decomposition rate of initiators are reaction temperature and solvents. In this process, free radical should find another radical for coupling. Then, radicals can get stabilized. Highly reactive free radical attacks the double bond of the monomer molecule. Double bonds are made up of two electrons. First one appears as sigma and second one appears as pi electrons. In initiation reaction, R-X plays role as an initiator, a metal complex (Mtn) goes through a one-electron oxidation and get a halogen atom from a starting species at the same time. An organic radical (R·) and a metal complex (Mtn+1) can be produced by this reaction. This process consists of the activation (kact) and deactivation (kdeact) rate constant. In ATRP, initiation should be complete and fast at low monomer conversion [27,28].
2. Propagation: In the second process of ATRP mechanism, the propagation of polymer chains occurs by adding new monomers to the growing chain ends. It is important to rapidly deactivate growing chains to obtain polymers with high quality. The explained condition is continuous until the end of process [28, 29].
3. Termination: this reaction is the last step of polymerization process with rate constant (kt) that is mainly through radical coupling and dis-proportionating in ATRP method. Only a small percent of polymer chains can reach and experience the termination reaction in a controlled ATRP [27,28]. This process can be separated into two different categories of coupling termination and dis-proportionating termination. The dis-proportional termination has shorter chain length than coupling termination.

In living polymerization systems, the chain ends must not be terminated at the end of the ATRP and they must be living to be usable as macroinitiators in further polymerization processes. To achieve this goal, all polymer chains should have a halogen atom at the end of the chain when the polymerization is completed. Then, they can be reused to obtain block copolymers or other advanced polymer architectures [27,28].

2.4 Process of Synthesizing Polymer/Colemanite Composites

Various methods for fabrication of polymer composites are such as; a) solution mixing, b) melt compounding and c) in-situ polymerization that are in use to produce polymer/colemanite composites. Same as the other types of polymer composites, the dispersion and distribution of colemanite in polymer matrix are very important during the synthesize of polymer/colemanite composites. Due to this fact, the most appropriate method must be used to obtain the effective dispersion and distribution [30,31].

2.4.1 In situ polymerization method

In this method of polymerization, monomer and colemanite filler should be mixed in first step. It allows the interaction between the monomer and filler (particles). After the occurrence of homogeneous mixture, initiator is added and polymerization is initiated after the monomer intercalation. Heat accelerates the polymerization process. The general in-situ polymerization is presented below (Figure 2.4)

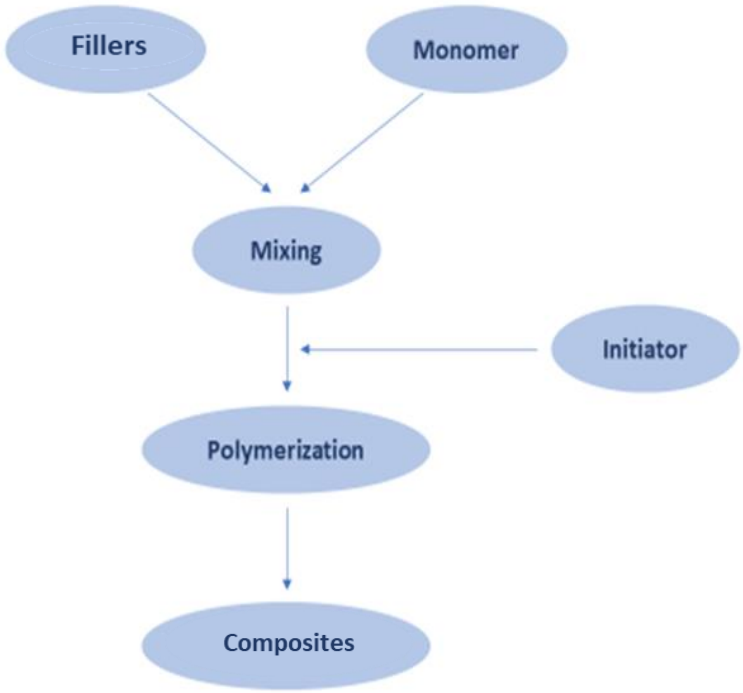

Figure 2.4 : Diagram of in-situ polymerization process.

Compared to the other methods, the in-situ polymerization has outstanding performance. This method of polymerization improves the dispersion and distribution

of layered colemanite-filler in matrix. Compared to composites synthesized by melt mixing or solution mixing, the synthesized composites by this method have superior performance [32,33].

2.4.2 Process of mixing the solution

Solution mixing is a common technique to prepare polymer composites. This method has an extensive use because of its simple operation process. First, the solid polymer is dissolved in a chemical solvent, and then mixed with the dispersed filler in the same solvent by stirring or sonication. Consequently, the effective interaction between polymer molecules and the colemanite layers occurred. Polymers form the composites after removing the solvent with evaporation. This method has both advantages and disadvantages. Its advantage is to work very well with small sample sizes. Also, this polymerization method has consistent dispersion. The schematic representation of the explained synthesis technique is shown below (Figure 2.5).

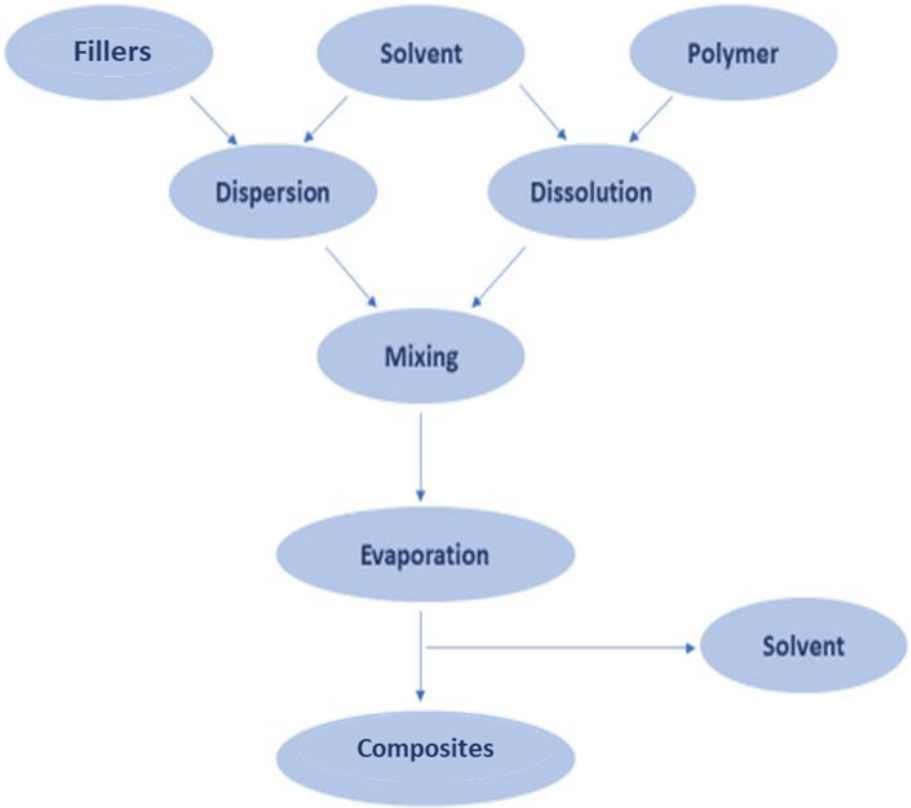

Figure 2.5 : Process of solution mixing.

Some disadvantages of this method are such as the necessity to use chemical solvent and sonication for mixing the colemanites with the polymer suspension. The other problem is that the available organic solvents are limited. In addition, environmental effects are a result of using solvent in large quantities [30,31,32].

2.4.3 Process of melt compounding

Melt compounding is on of useful techniques to produce large-scale polymer composites, thermoplastic polymers and fillers. This technique can't be utilized at low compositions based on the fact that their aspect ratios are high. Direct combination of colemanites into the molten or viscous polymer takes place in the polymerization process of this method. The solid polymer can be softened by high temperature. This high temperature also can cause the easy dispersion of colemanites.

However, this is not an effective method to disperse colemanites in molten polymer or viscous polymer, especially in the case of preparing higher concentration of colemanite.

The disadvantage of this method is to limit the potential nanoscale reinforcement ability. In this method, the mechanical and electrical performance of the obtained composite are limited too. Thus, the melt compounding method results in poor dispersion of colemanite in polymer matrix, compared to in situ polymerization and solution mixing [30,31,32]. The process of melt compounding technique is shown in Figure 2.6.

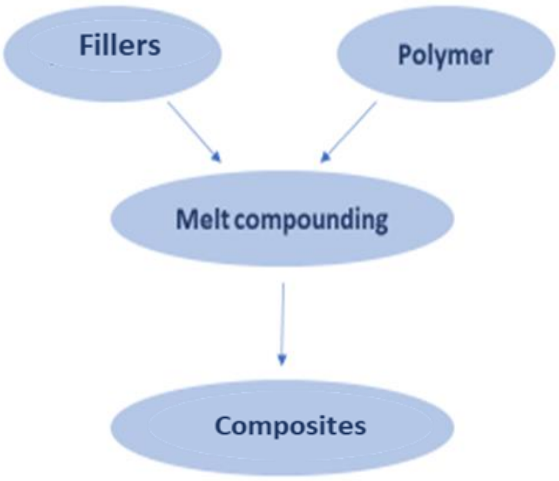

Figure 2.6 : Process of melt-compounding.

2.5 Gamma Radiation Transmission

Gamma rays are photons with high energies about 10000 times more than energy of visible photons and wavelengths shorter than 10-11 m. The decay of nucleus from a state with high-energy to another state with lower energy leads to the production of gamma rays. This process is called gamma decay. Gamma photons have no mass and electrical charge. Thus, they can only cause indirect ionization. Gamma ray is a highly penetrating electromagnetic radiation [34].

These rays pass through materials and interact with them in different ways. This is a complex process and there are a variety of interactions that can occur between the gamma radiation and material but there are three important interactions that have high probability of occurrence. These interactions are mentioned below [35,36]:

1. In photoelectric event, γ-ray interacts with an inner electron of atom, then the incident photon loses all of its energy and disappears. This interaction occurs at low energies of gamma rays. A part of its energy overcomes the binding energy of electron and the rest is transferred to ejected electron as kinetic energy. The energy of photoelectron can be calculated from equation below:

$$E_e = h\upsilon - E_b \quad (2.1)$$

Where, hυ is the energy of incident photon, Eb is the binding energy of electron and Ee is the energy of photoelectron. Photoelectric absorption occurs when Eγ >Eb [35,36].

The photoelectric interaction is presented in Figure 2.7.

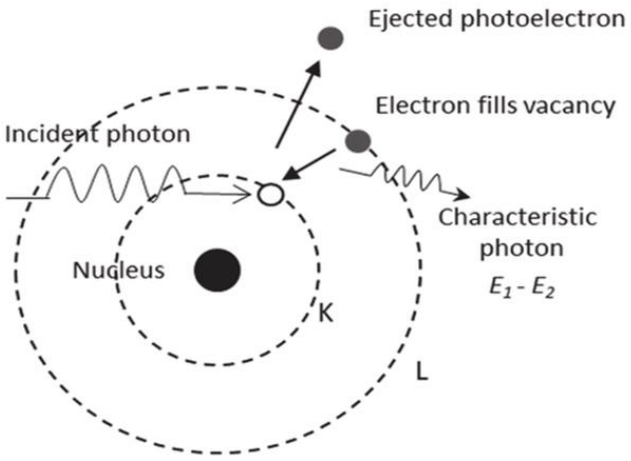

Figure 2.7 : Illustration of photoelectric effects.

2. In compton scattering process, the coming gamma ray interacts with target electron (Eγ >>Eb) in the atom and transfers a part of its energy to the recoiled electron. Different angles of scattering are possible in this event. Thus, transferred energy has a range that changes from zero to the energy values of incident photon. This interaction results in deflection of electron from the atom with a scattering angle and a decrease in the energy of the photon [35,36].

The Compton scattering process is presented below (Figure 2.8).

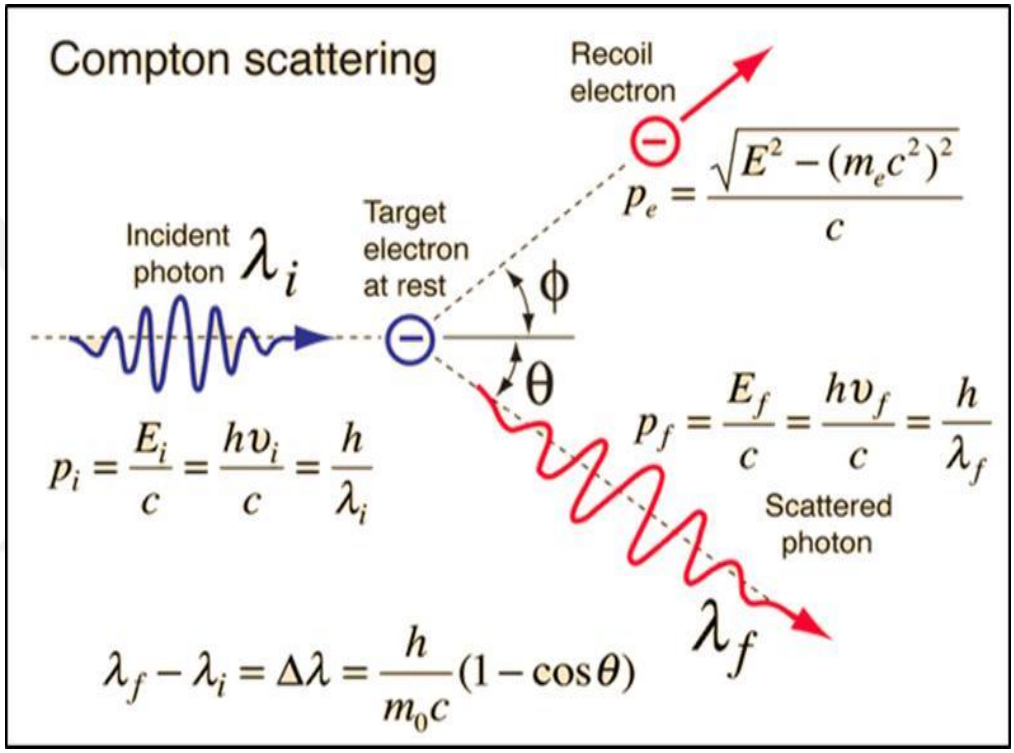

Figure 2.8 : Compton scattering.

3. Pair Production occurs when incident photon with energy twice the rest mass of the electron (at least 1.022 MeV) passes near the nucleus and interacts with electric field of nucleus. As the result of this electric field, pair production occurs which is the transformation of photon into a positron and an electron. The formed electron and positron of pair production are slowing down inside material and lose their kinetic energy. Then the combination of the electron and the positron through annihilation process results in the emission of two gamma photons, each has energy of 0.511 MeV. This is a common interaction in the case of materials with high atomic number [35,36]. The pair production interaction is presented in Figure 2.9.

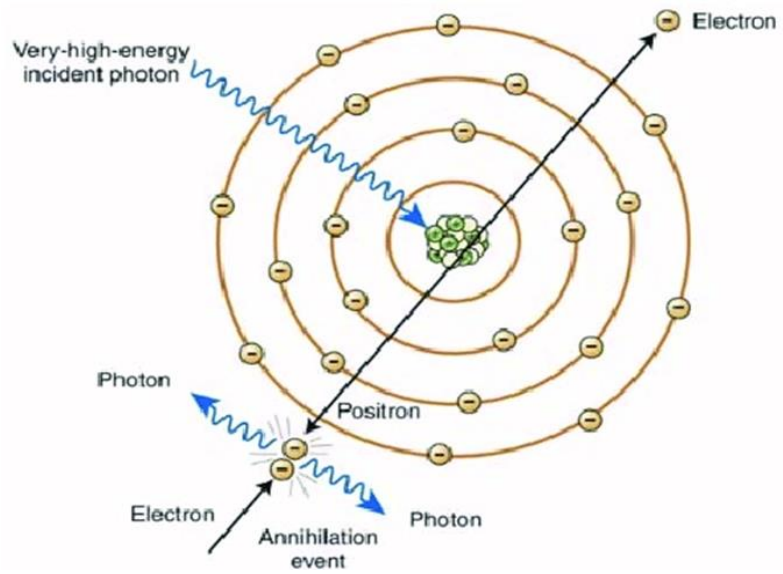

Figure 2.9 : Pair production process.

Probability relationship for these interactions can be obtained by the use of quantum mechanics. It shows the probability of each interaction, which is defined as absorption coefficient or cross section of interaction. The cross section of interaction and the intensity of gamma-ray determine the amount of attenuation when rays pass through the polymer material. The sum of absorption coefficients for photoelectric effect, Compton scattering and pair production is equal to total attenuation coefficient (μ_l) calculated by equation below:

$$\mu l\ (cm^{-1}) = \mu_{ph} + \mu_{co} + \mu_{pp} \qquad (2.2)$$

In this equation, μ_{ph} is the defined absorption coefficient for photoelectric effect, μ_{co} determines absorption coefficient of Compton scattering and μ_{pp} gives absorption coefficient of pair production [34].

Lambert-Beer equation determines the γ-ray attenuation inside the material.

$$I = Io\ e^{-(\mu l\ x)} \qquad (2.3)$$

I is the intensity of radiation passes through absorber material with thickness of x (cm). Io is the initial radiation intensity without any sample material. The gamma radiation transmission of composite sample is given by ratio I/I_o. In this equation, μ is linear attenuation coefficient and it dependent on gamma-ray energy, density and atomic number of sample material. Gamma-ray transmission decreases by the increase of absorber thickness. On the other hand, transmission increases by the increase of

gamma-ray energy. Mass attenuation coefficient is another useful expression that can be defined as the ratio of linear attenuation coefficient to density (μ/ρ) and has unit of area per unit mass (cm^2/g). [35].

2.6 Neutron Transmission

Neutron is a subatomic particle that derives its name from the fact that it is neutral; it has no electrical charge. Neutron is extremely dense and mass of it is slightly greater than the mass of proton. All atomic nucleuses have at least one neutron except hydrogen. Protons and neutrons come together with nuclear force for the formation of atomic nuclei. Neutrons are composed of two down and one upward quartz [42].

The classification of neutrons based on their energies is given below:

a) cold and ultracold: E~meV~ μeV

b) Thermal/slow: E ~ kT~1/40 eV

c) Epithermal: 100 keV >E >0.1 eV

d) Fast: 10-20 MeV > E >100-200 keV

e) High-energy: E>100 MeV

Neutrons interact with matter in different ways. When neutron interacts with a nucleus, five reactions are possible to occur (Figure 2.10).

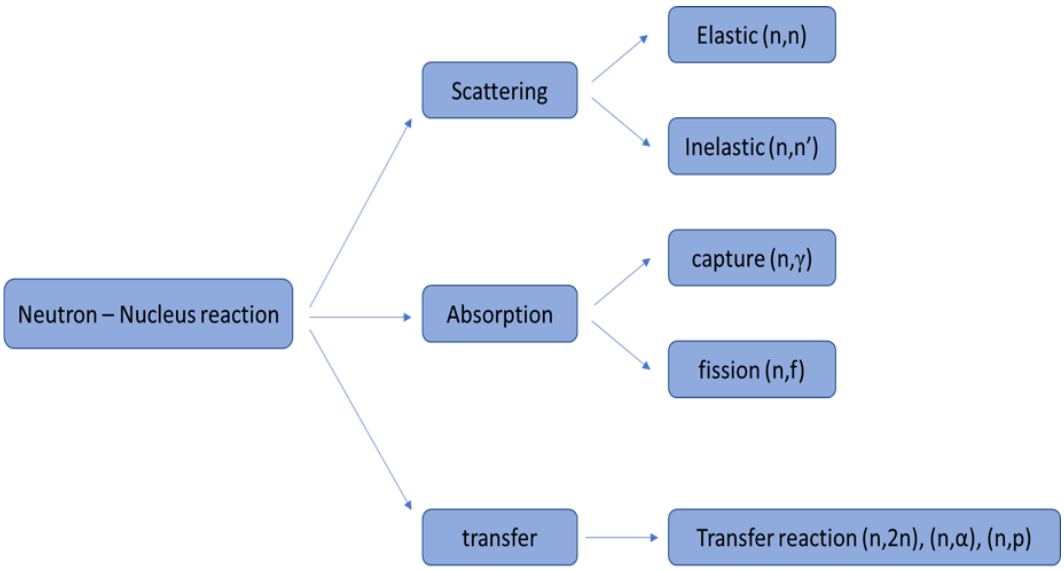

Figure 2.10 : Neutron-Nucleus interactions.

Elastic scattering: Neutrons transfer a part of their energy to the nucleus in this collision and then they separate to different directions. Target nucleus receives energy and moves faster.

Inelastic scattering: A neutron may be temporarily absorbed when it hit the nucleus. As the result, the compound nucleus appears. This compound nucleus is excited and can turn back to initial state by the emission of another neutron with lower energy along with emission of a gamma photon [43].

Neutron Absorption: These reactions occur when neutron is completely absorbed. The formation of compound nucleus takes place at the end of the reactions. This group of reactions occur in nuclear reactors.

Two main absorption reactions can be classified as below:

1. Radiative Capture: It is the only possible absorption reaction to occur in case of non-fissionable nuclei. In this reaction, incident neutron is fully absorbed and formed compound nucleus decays to its initial state of energy by emission of gamma. Thus, capture reaction results in the loss of a neutron coupled with emission of one or more gamma rays. Its cross-section is presented by σ_γ.
2. Neutron-induced Fission: A neutron can be absorbed or can cause a nuclear fission in the case of fissionable materials. Due to this, the absorption cross section can be given as: $\sigma_a = \sigma_\gamma + \sigma_f$.

Neutron transfer: In this type of reactions, neutron can be absorbed in order to produce compound nucleus. Compound nucleus can emit different charged particles such as a photon or maybe an alpha particle. At the end, a nucleus of a different element appears. Neutron transfer group of reactions are; (n, 2n), (n, α), (n, p).

The total probability for the interaction of neutron with material is the sum of cross sections for all interactions explained earlier. Attenuation coefficient value for neutrons can be obtained from equation below:

$$I = Io\, e^{-\Sigma(tot).x} \tag{2.4}$$

Where, Σ_{tot} is the total macroscopic cross-section of neutrons, Io is the initial intensity and I is the measured intensity after passing through the absorber material with thickness of x.

2.7 Beta Transmission

In this experiment, the emission of beta particles was together with the emission of Bremsstrahlung radiation which is produced from the deceleration of a charged particle, typically an electron at Coulomb interaction. In the case of materials with high Z number, there is a more intense production of Bremsstrahlung radiation when negative beta particles interact with material. Thus, using low Z number materials is more appropriate to reduce the intensity value of Bremsstrahlung radiation in the experiments [37].

The changes in relative intensity value (I/Io) of beta radiation were calculated for pure PMMA and PMMA/Colemanite composite samples by using equation below:

$$I = Io\, e^{-(\mu x)} \tag{2.5}$$

When, I_o is the initial intensity, I is the transmitted intensity passed through material and x is the thickness of sample material. Linear attenuation coefficient value in this equation is presented by μ.

3. EXPERIMENTALS

3.1 Used Chemicals

The used materials were; a) Tetra-n-butylammonium bromide (Bu4NBr), b) 98+% (Alfa Aesar), c) Copper bromide (CuBr), d) Puratronic®, e) 99.998% (metals basis) (Alfa Aesar), f) Methyl methacrylate (MMA), g) 99%, stab.(Alfa Aesar), h) 1,1,4,7,7-Pentamethyldiethylenetriamine (PMDETA), i) 98% (Alfa Aesar), j) Ethyl 2-bromoisobutyrate (EBiB), k) 98+% (Alfa Aesar), l) pure argon, m) regulator and n) Colemanite filler.

3.2 Preparation of PMMA/Colemanite Composite Samples

In this experiment, all the preparations and measurements were performed in two hands AtmosBag at ITU Prof.Dr. Adnan Tekin Materials Science and Production Technologies Applied Research Center (ATARC).

First, the chemical materials and tubes together with a magnetic mixer were placed inside this AtmosBag (Figure 3.1). Before the measurements, the Atmosbag was vacuumed. Then the system was filled with pure argon. The chemicals weighting process was performed in the argon atmosphere of AtmosBag.

Figure 3.1 : The chemicals weighting in AtmosBag.

For the preparation of base samples, Bu4NBr of 1.211 g and 3.76 mmol as solvent together with CuBr of 0.067 g and 0.47mmol as catalyst were weighted and for composite samples, extra colemanite concentrations of 15 %, 30 %, 40% were added to tubes and placed inside AtmosBag. Measurements of chemicals were performed using Precision Libra. After the measurements, tubes were sealed and taken out from the AtmosBag in order to put them in another AtmosBag for synthesis process (Figure 3.2). The prepared MMA of 28.2 g and 0.282 mol was added to the tubes and mixed with chemicals via gas tight syringe. Then, PMDETA of 0.081 g and 0.47mmol as ligand was added to mixtures. Then, mixtures were degassed using pure argon for about 3 minutes. At last, EBIB of 0.092g and 0.47 mmol as initiator was added to tubes in order to start polymerization process.

Figure 3.2 : The synthesis process performed in the AtmosBag.

All the tubes were taken out of the AtmosBag, closed and sealed with parafilm. Then, tubes were put on a magnetic stirrer with adjustable temperature property to complete the polymerization process (Figure 3.3).

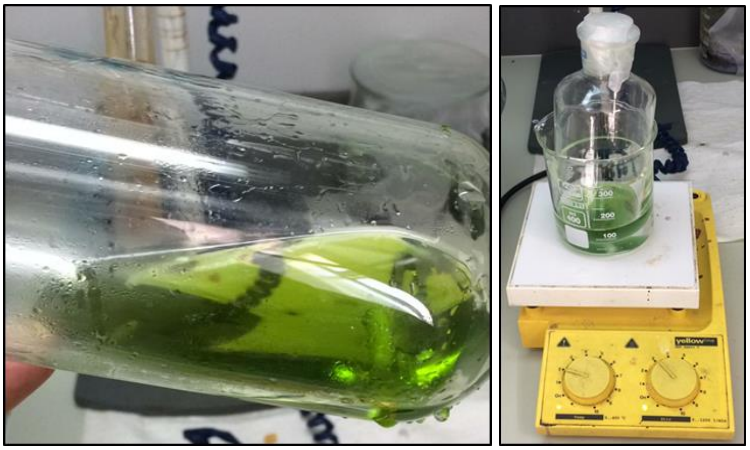

Figure 3.3 : The completion of polymerization process with magnetic stirrer.

Images of base PMMA and PMMA/colemanite composite samples were presented below (Figure 3.4).

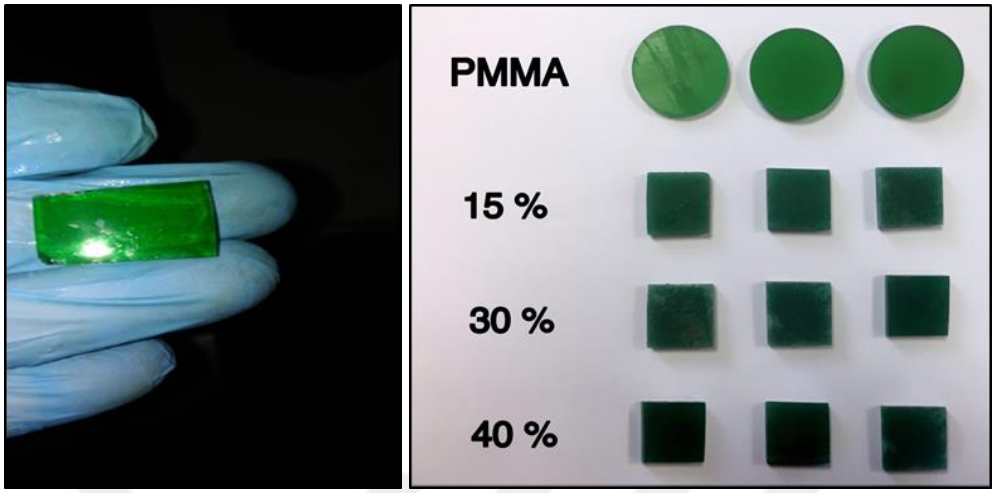

Figure 3.4 : Prepared base PMMA and PMMA/Colemanite composite samples.

3.3 Application of Cs-137 and Co-60 Radioisotopes in Gamma Transmission Technique

Cs-137 and Co-60 radioisotopes with different gamma photon energies were utilized as gamma sources in gamma transmission method to calculate attenuation coefficient values for PMMA/colemanite composites. The Cs-137 radioisotope with the half-life of 30.1 years and a single peak of gamma that appears at the energy of 0.662 MeV (Figure 3.5). The Co-60 radioisotope has the half-life of 5.23 years which is short compared to Cs-137 (Figure 3.6). It shows two peaks of gamma at energies of 1.17 MeV and 1.33 MeV. The relation between linear attenuation and colemanite content can be determined by the use of these gamma radioisotopes [38].

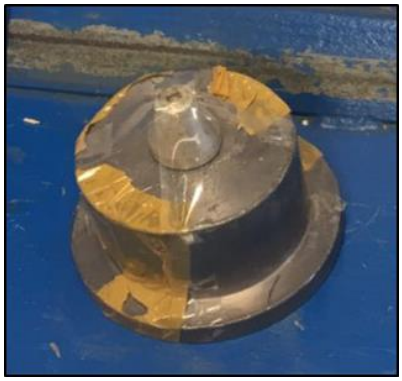

Figure 3.5 : The image of Gamma source (Cs-137 radioisotope).

Figure 3.6 : Images of the Gamma source (Co-60 radioisotope).

The gamma rays that can pass through material are measurable using gamma transmission method. Detector and gamma source were placed face-to-face on the opposite sites of the same-axis, presented in Figure 3.7.

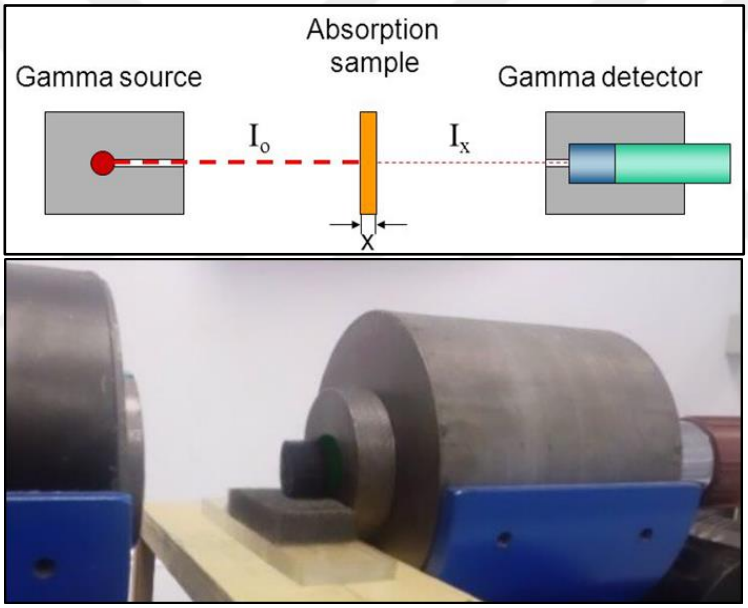

Figure 3.7 : The experimental set up for gamma transmission technique.

The linear attenuations were measured for samples by using gamma spectrometer that contains a detector (Canberra Bicron of Model: 802-2X2) and it was connected to a Multi-Channel Analyzer with 1024 channels.

The diameters of both Cs- 137 and Co-60 radioisotopes were 6mm. The thickness of lead collimator was 10 mm and collimator hole had 7mm diameter. The diameter of used detector was 20 mm. The source-detector distance was 160 mm during all measurements. Collimator was used to focus radiation intensity into detector. The source-sample distance was maintained 110 mm.

The intensity of the intensity coming gamma rays from the source were measured by detector. First, the initial baseline (I_0) was measured, which is the intensity of the atmosphere without using any composite material. Then, the PMMA/colemanite composites were placed in the distance between source and detector. Gamma intensity was measured for 15 minutes per PMMA/colemanite composite sample. In order to calculate the mean values, all of the measurements were performed at least three times in the same parameters. This experiment was performed in Radiation Applications Laboratory-B of ITU Energy Institute.

3.4 Application of Neutron Howitzer (NH3) with Pu-Be Neutron Source

This Neutron Howitzer (NH3) contains 239Pu-Be neutron source (α, n), neutron collimator, neutron detector and neutron shielding equipment used in experiments for neutron transmission measurements. Table 3.1 gives the characteristics of ^{239}Pu-Be neutron source containing Neutron Howitzer [44].

Table 3.1: Characteristics of Neutron Howitzer (NH3) with ^{239}Pu-Be neutron source.

Properties	Value
Neutron Source	Pu-Be Neutron Source
Neutron Source Type	Nuclear Chicago Corporation
Neutron Production Reaction	(α,n)
Average Neutron Energy	53.97 kJ/mole
Neutron Flux	10^4 n/cm^2 s
Activity	2 Ci
Number of the Irradiation Ports	2
Thickness of the paraffin	25 cm
Sizes of the Howitzer	Ø 60 cm x 90 cm

Two radial beam ports of neutron howitzer are 29 cm long and have the diameter of 5 cm. One Port is used for thermal neutrons and it is utilized to calculate total macroscopic cross section for various materials such as polymeric materials. The other port is used for epithermal neutrons. It is utilized to calculate effective cross section for denser materials.

Pu–Be neutron source has average neutron energy of 5 MeV with activity of 5 Ci and the neutron howitzer generates neutron flux (at 106 n/cm^2). Insignificant amount of fast and epithermal scattered neutrons was received from port and thermalized, then

absorbed by the hydrogen and carbon content at paraffin wax of NH3. Samples were examined by thermal slow neutrons with energy of 0.025 eV.

Changes in values of total macroscopic cross sections for PMMA/Colemanite composites were evaluated by using Thermal neutron port of NH3 (Figure 3.8).

Figure 3.8 : Port of the used Neutron Howitzer.

This experiment was performed in the Neutron Howitzer at ITU Energy Institute (Figure 3.9). Neutron attenuation property of PMMA/colemanite composites was examined by the rise of colemanite amount in composite.

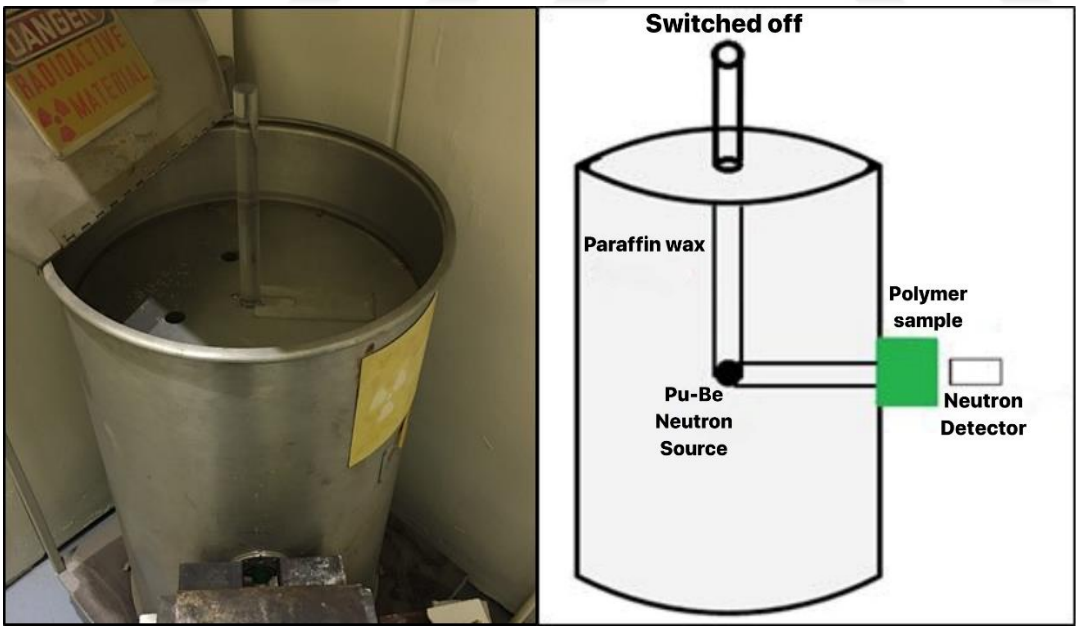

Figure 3.9 : The used Neutron Howitzer.

In the first step, initial count (I_o) was measured. Then, the PMMA/colemanite composite samples with determined thicknesses were placed in experimental setup.

Duration of count measurements were 90 seconds for each sample. Each count was repeated at least three times to calculate mean value.

3.5 Application of Sr-90 Radioisotope in Beta Transmission Test

Beta transmission test is usable for thickness measurements in industry. This method is useful in control processes for polymers and ensures the assessment of the density changes [39]. Sr-90 radioisotope has the activity of 3.58 mCi and the half-life of 28.1 years. This radioisotope emits beta particles at energy of 0.546 MeV. Yittrium-90 radioisotope with 64 h half-life appears from the decay of Sr-90 and emits beta particles. It emits high-energy beta radiation (2.28 MeV).

In this study, the experimental settlement was prepared in order to determine the beta attenuation of PMMA/Colemanite composite samples. The used beta source in this experiment was Sr-90 of 2.86 mCi with radius of 0.015 cm and max electron energy of 0.546MeV (Figure 3.10). Beta measurements were performed in a cell made of plexiglass.

Figure 3.10 : The used beta source (Sr-90).

In beta transmission test, half-life of the source and its energy can be considered as important parameters in evaluation of radiation penetration.

In this experiment, survey meter was performed dependent on its high counting efficiency. This survey meter is a high-quality Geiger-Muller type of detector in use for X-ray and gamma measurements which is a suitable choice for protection from radiation and health physics applications [40].

The produced Bremsstrahlung radiation was considered as X-ray. The changes of beta intensity were studied considering Bremsstrahlung radiation. In this experiment, there

was the emission of Bremsstrahlung radiation as X-ray together with the emission of beta particles from Sr-90 and its decay product Y-90. In measurements, the emitted X-ray was eliminated and the counts were taken by detector only for the emission of beta particles. In order to have an acceptable electron beam and eliminate electron scattering, a special polymer collimator was used in this experiment. This collimator had outer and inner diameters of 13 cm and 6 cm.

4. RESULT AND DISCUSSION

4.1 Gamma Transmission Measurements

By the use of Cs-137 and Co-60 radioisotopes as two different sources of gamma, the changes in relative intensity for PMMA/Colemanite composite samples were defined as a function of sample thickness. Therefore, it became possible to determine the changes in values of attenuation coefficient (μ) for pure PMMA and PMMA/Colemanite composites samples at different colemanite concentrations and sample thicknesses.

At the end of the measurements, values of linear attenuation coefficients (μ) for gamma sources (Cs-137 and Co-60 radioisotopes) were obtained from the thicknesses versus relative counts graphs.

4.1.1 Gamma transmission measurements using Cs-137

The changes of relative intensity values for pure PMMA with the rise of the thickness using Cs-137 as gamma source were listed below (Table 4.1). The linear attenuation coefficient results were given in Figure 4.1.

Table 4.1: Results of gamma transmission measurements for pure PMMA using gamma source (Cs-137).

Thickness (cm)	Count 1	Count 2	Count 3	Average Count	Standard Deviation	Relative Count (I/Io)
0	3258	3270	3285	3271.000	0.003377	1.00000
0.5	2980	3085	3050	3038.333	0.013345	0.92886
1	2889	2851	2980	2906.667	0.005065	0.88861
1.5	2675	2827	2875	2792.333	0.019814	0.85366

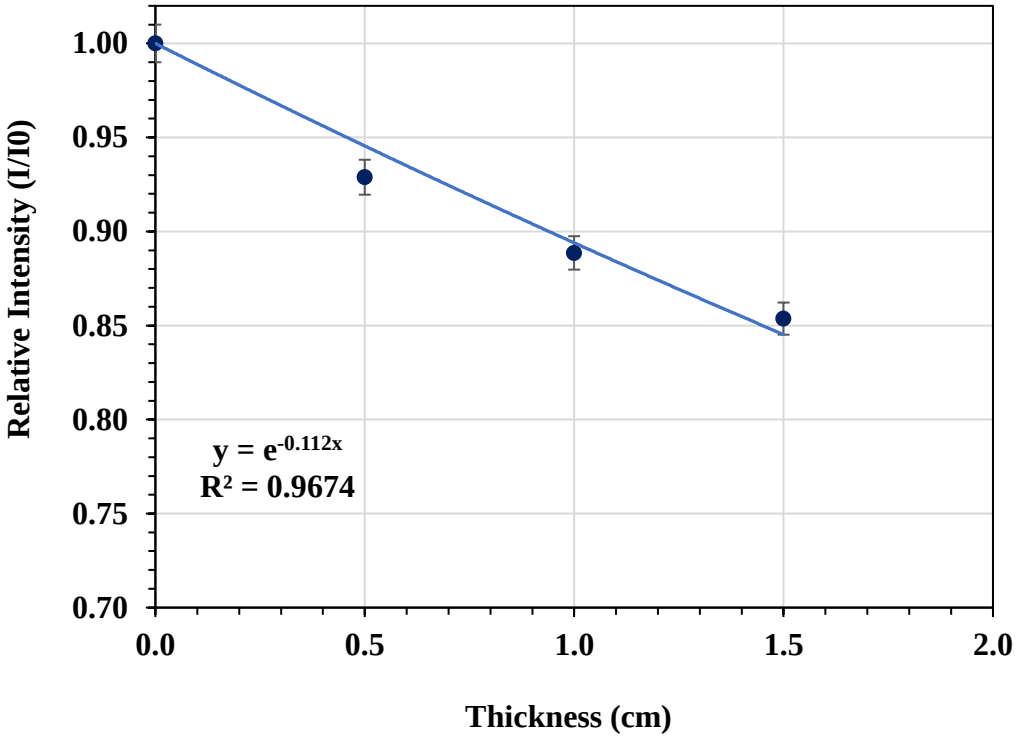

Figure 4.1 : Graph of relative intensity-thickness for pure PMMA using gamma source (Cs-137).

Results of gamma transmission measurements for examined samples at 15 % colemanite concentration using Cs-137 radioisotopes were listed below (Table 4.2).

Changes in relative intensity of PMMA/Colemanite 15 % samples by the rise of thickness were given in Figure 4.2. It also represents the linear attenuation coefficient.

Table 4.2: Results of gamma transmission measurements for PMMA/Colemanite 15 % samples using gamma source (Cs-137).

Thickness (cm)	Count 1	Count 2	Count 3	Average Count	Standard Deviation	Relative Count (I/Io)
0	3258	3270	3285	3271.000	0.003377	1.00000
0.5	2985	2976	2992	2984.333	0.002002	0.91236
1	2841	2815	2796	2817.333	0.005639	0.86130
1.5	2726	2778	2671	2725.000	0.013356	0.83307

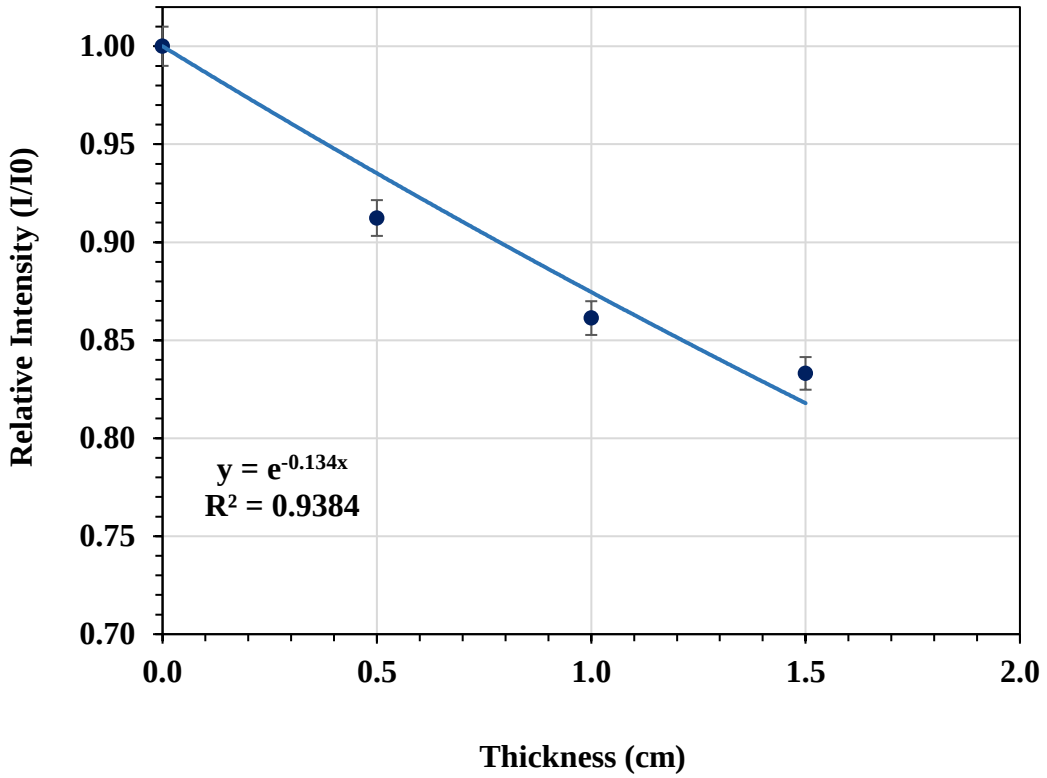

Figure 4.2 : Graph of relative intensity-thickness for PMMA/Colemanite 15 % samples using gamma source (Cs-137).

Results of gamma transmission measurements for PMMA/Colemanite 30 % samples using Cs-137 as gamma source were presented below (Table 4.3). Linear attenuation coefficient can be seen in Figure 4.3.

Table 4.3: Results of gamma transmission measurements for PMMA/Colemanite 30 % samples using gamma source (Cs-137).

Thickness (cm)	Count 1	Count 2	Count 3	Average Count	Standard Deviation	Relative Count (I/Io)
0	3258	3270	3285	3271.000	0.003377	1.00000
0.5	2960	2862	2886	2902.667	0.012751	0.88739
1	2597	2759	2758	2704.667	0.023275	0.82686
1.5	2610	2567	2625	2600.667	0.007515	0.79506

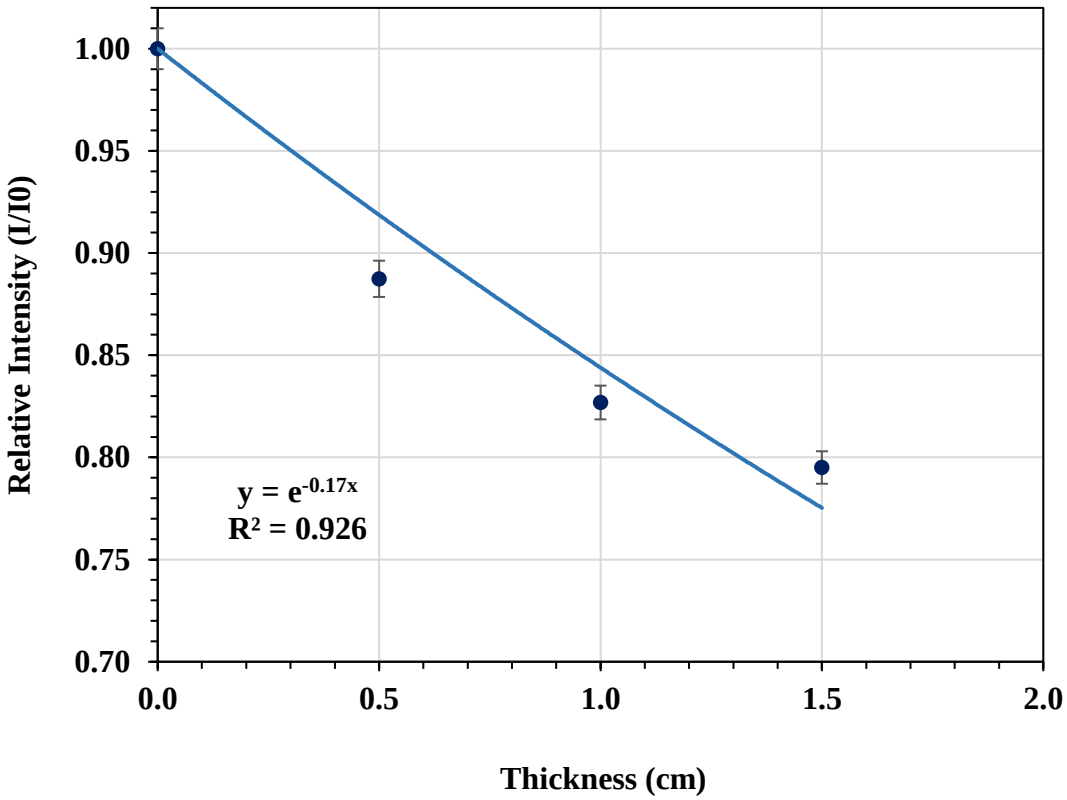

Figure 4.3 : Graph of relative intensity-thickness for PMMA/Colemanite 30 % samples using gamma source (Cs-137).

Results of gamma transmission measurements for PMMA/Colemanite 40 % samples using Cs-137 were listed below (Table 4.4). Linear attenuation coefficient was presented in Figure 4.4.

Table 4.4: Results of gamma transmission measurements for PMMA/Colemanite 40 % samples using gamma source (Cs-137).

Thickness (cm)	Count 1	Count 2	Count 3	Average Count	Standard Deviation	Relative Count (I/Io)
0	3258	3270	3285	3271.000	0.003377	1.00000
0.5	2850	2937	2834	2873.667	0.013836	0.87852
1	2610	2736	2690	2678.667	0.015916	0.81891
1.5	2528	2462	2549	2513.000	0.009512	0.76826

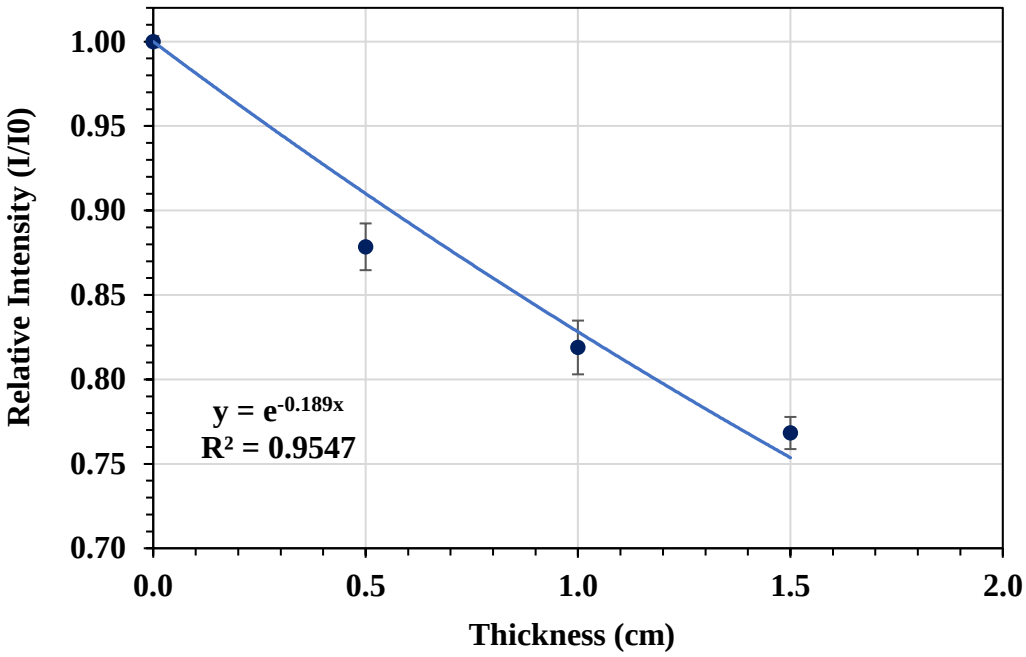

Figure 4.4 : Graph of relative intensity-thickness for PMMA/Colemanite 40 % samples using gamma source (Cs-137).

Theoretical mass attenuation coefficients were evaluated with XCOM program by using the chemical compositions of samples in the calculations (Figure 4.5).

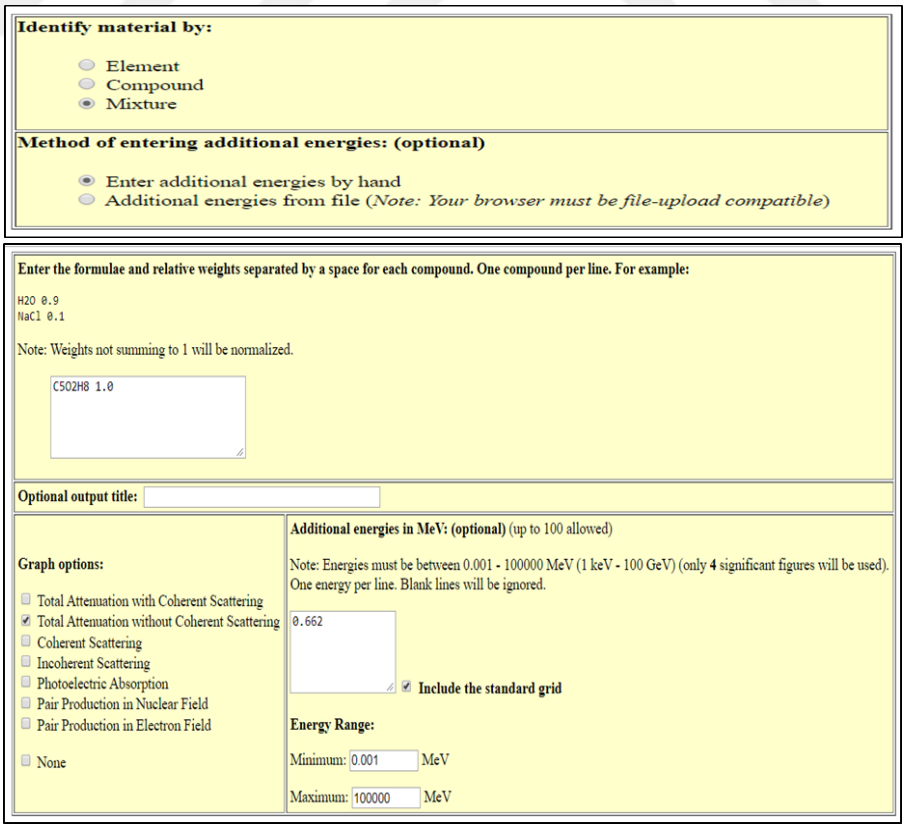

Figure 4.5 : Calculation of theoretical mass attenuation coefficient using XCOM program.

The values for linear attenuation coefficients were obtained from the experimental results and presented in prepared graphs based on sample thicknesses versus relative counts.

Pycnometer measured the changes in density of prepared samples by the rise of colemanite concentration. Then, the values of mass attenuation coefficients were determined from $\mu_m = \mu_l/\rho$. Theoretical and experimental results were compared below (Table 4.5).

Table 4.5: Comparison of theoretical and experimental results for gamma source (Cs-137).

Samples	Linear attenuation coefficients μ (cm^{-1})	Density ρ (g/cm^3)	Mass attenuation coefficients μ/ρ (cm^2/g)	Theoretical mass attenuation coefficients μ/ρ (cm^2/g) (XCOM)	Difference (%)
PMMA	0.112	1.110	0.10090	0.10310	2.1
15 %	0.134	1.216	0.11019	0.11370	3.0
30 %	0.170	1.232	0.13798	0.14270	3.3
40 %	0.189	1.247	0.15156	0.16390	7.5

Based on the results presented in Table 4.5, linear and mass attenuation coefficients increased with the rise of the colemanite concentration in the PMMA/colemanite composite samples.

Results determined that theoretical mass attenuation coefficients are greater than experimental mass attenuation coefficients. The calculated difference between theoretical and the experimental results indicated that the obtained values were in acceptable ranges.

The results of gamma radiation attenuation at different colemanite concentrations for PMMA/colemanite composite samples against Cs-137 radioisotope were compared in Figure 4.6.

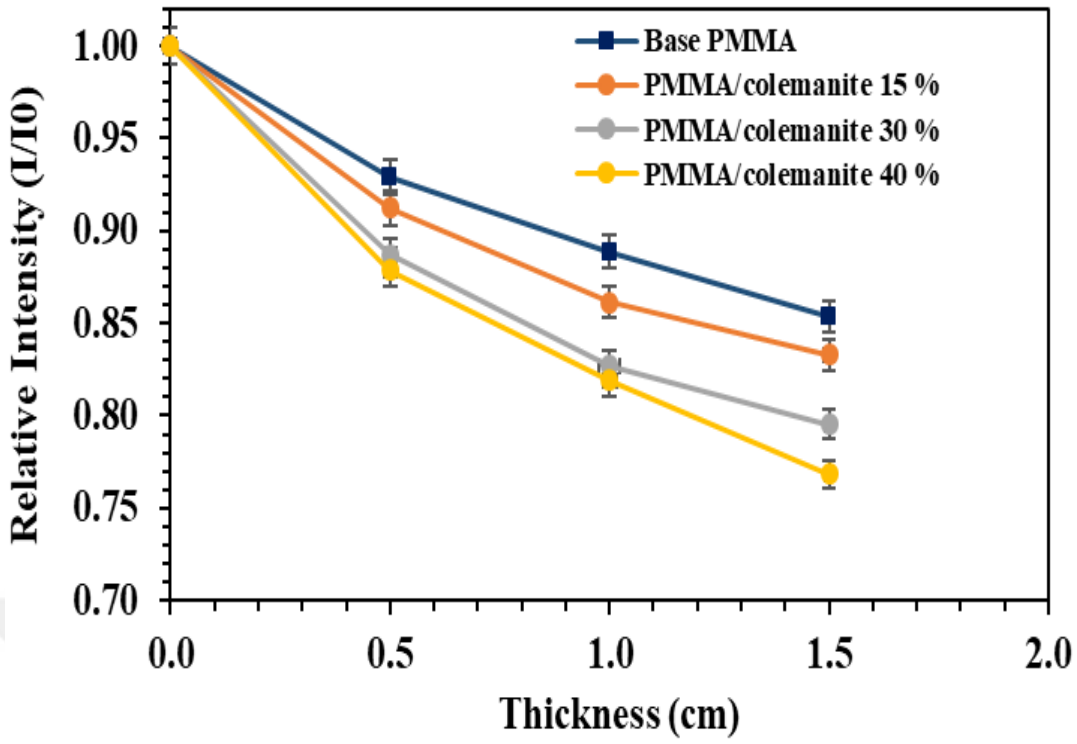

Figure 4.6 : Comparison of gamma radiation attenuation at different colemanite concentrations for Cs-137 radioisotope.

4.1.2 Gamma transmission measurements using Co-60

Results of gamma transmission measurements for base PMMA samples using Co-60 at 1.17 MeV gamma-peak were listed below (Table 4.6). Linear attenuation coefficient was shown in Figure 4.7.

Table 4.6: Results of gamma transmission measurements for pure PMMA using Co-60 radioisotope (at 1.17 MeV).

Thickness (cm)	Count 1	Count 2	Count 3	Average Count	Standard Deviation	Relative Count (I/Io)
0	3623	3490	3477	3530.000	0.018690	1.000000
0.5	3412	3234	3260	3302.000	0.022239	0.935411
1	3164	3176	3129	3152.500	0.005648	0.893059
1.5	3016	2954	3158	3042.667	0.024190	0.861945

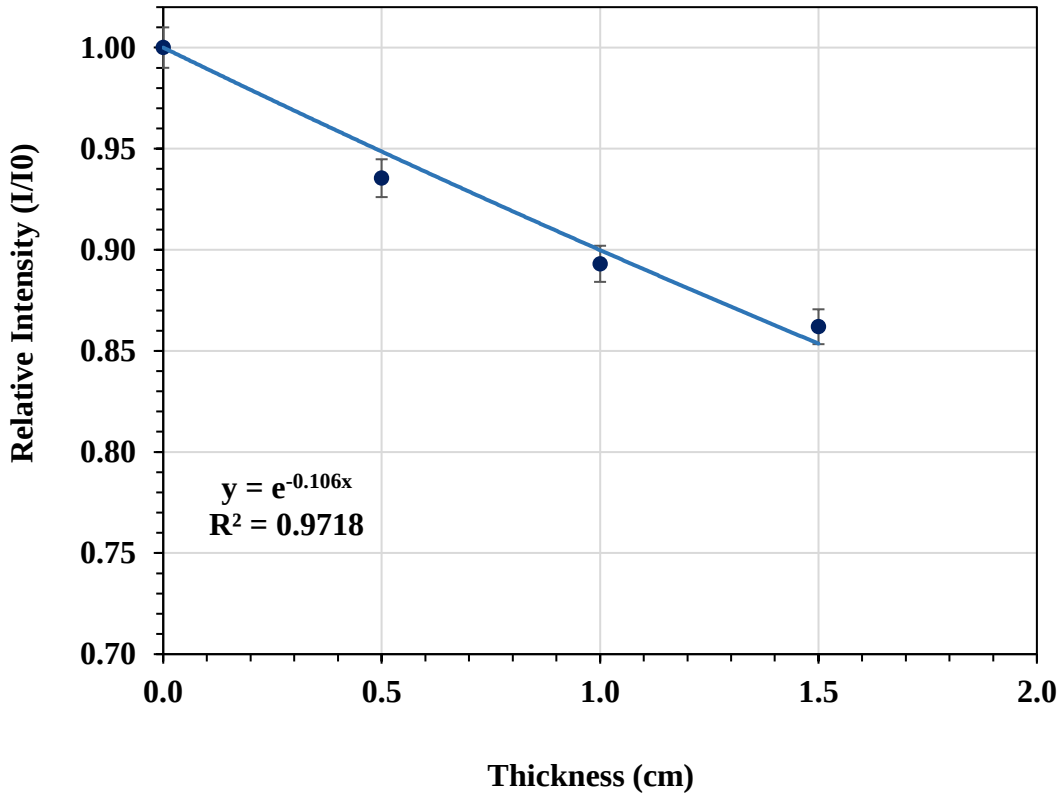

Figure 4.7 : Graph of relative intensity-thickness for pure PMMA using Co-60 radioisotope (at 1.17 MeV).

Result of gamma transmission measurements for PMMA/colemanite 15 % samples using Co-60 at 1.17 MeV gamma-peak were listed below (Table 4.7). Linear attenuation coefficient can be seen in Figure 4.8.

Table 4.7: Results of gamma transmission measurements for PMMA/Colemanite 15 % samples using Co-60 radioisotope (at 1.17 MeV).

Thickness (cm)	Count 1	Count 2	Count 3	Average Count	Standard Deviation	Relative Count (I/Io)
0	3623	3490	3477	3530.000	0.018690	1.00000
0.5	3392	3256	3227	3291.667	0.020376	0.932483
1	3103	3042	3063	3069.333	0.007168	0.869500
1.5	2928	2974	2937	3264.00	0.005639	0.834655

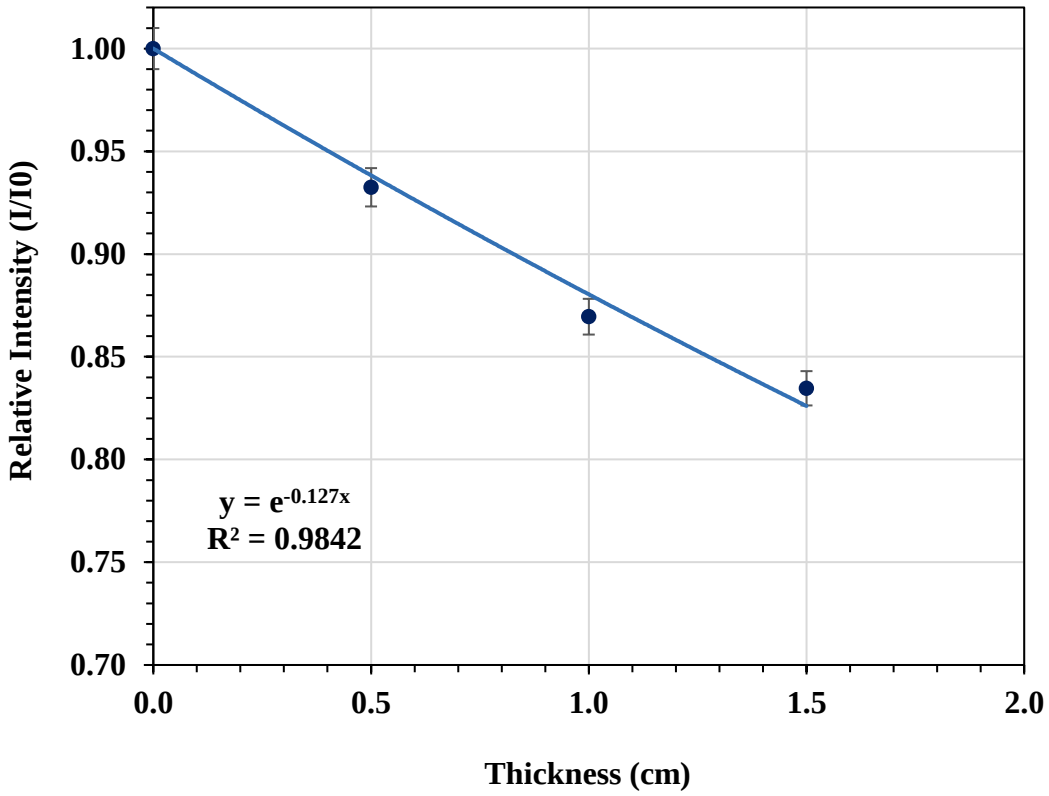

Figure 4.8 : Graph of relative intensity-thickness for PMMA/Colemanite 15 % samples using Co-60 radioisotope (at 1.17 MeV).

The obtained Results of gamma transmission measurements for PMMA/colemanite composite 30 % samples using Co-60 at 1.17 MeV gamma-peak were presented below (Table 4.8). Linear attenuation coefficient was calculated and presented in Figure 4.9.

Table 4.8: Results of gamma transmission measurements for PMMA/Colemanite 30 % samples using Co-60 radioisotope (at 1.17 MeV).

Thickness (cm)	Count 1	Count 2	Count 3	Average Count	Standard Deviation	Relative Count (I/Io)
0	3623	3490	3477	3530.000	0.018690	1.000000
0.5	3263	3253	3195	3237.000	0.008492	0.916997
1	3037	3049	2998	3028.000	0.006168	0.857790
1.5	2847	2939	2840	2874.333	0.012379	0.814259

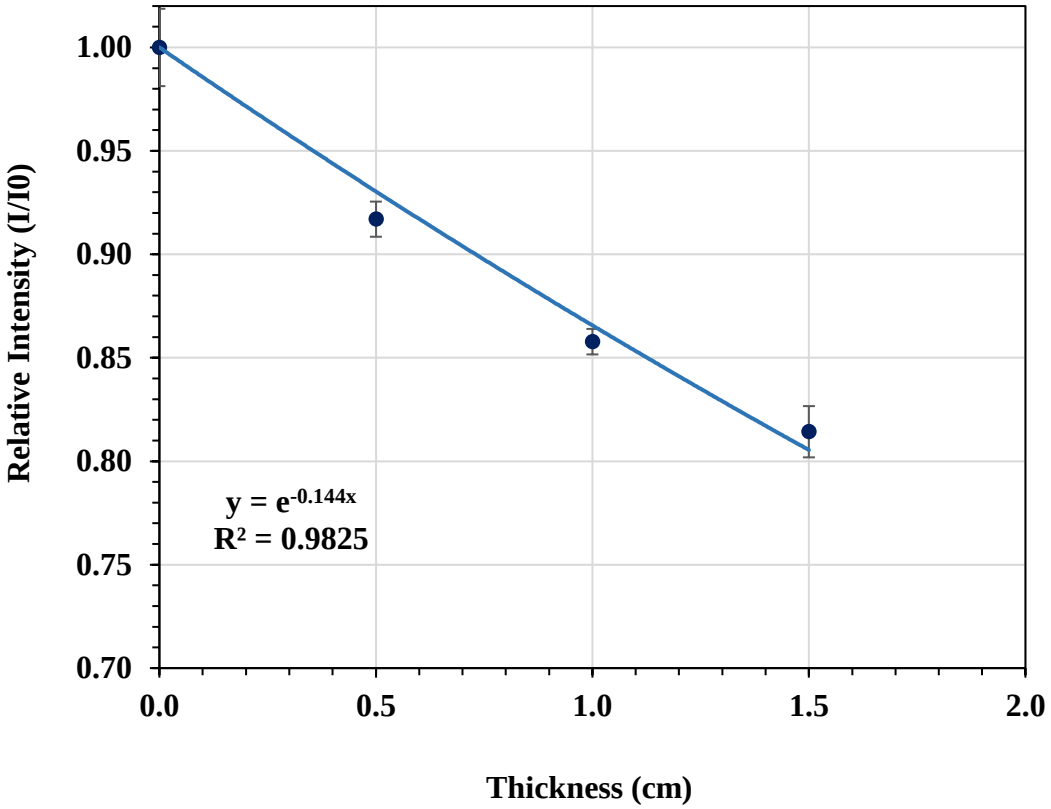

Figure 4.9 : Graph of relative intensity-thickness for PMMA/Colemanite 30 % samples using Co-60 radioisotope (at 1.17 MeV).

Results of gamma transmission measurements for PMMA/colemanite 40 % samples using Co-60 radioisotopes at 1.17 MeV gamma-peak were listed below (Table 4.9). Linear attenuation coefficient can be found in Figure 4.10.

Table 4.9: Results of gamma transmission measurements for PMMA/Colemanite 40 % samples using Co-60 radioisotope (at 1.17 MeV).

Thickness (cm)	Count 1	Count 2	Count 3	Average Count	Standard Deviation	Relative Count (I/Io)
0	3623	3490	3477	3530.000	0.018690	1.000000
0.5	3250	3165	3173	3196.000	0.010856	0.905382
1	2922	2973	2977	2957.333	0.007093	0.837771
1.5	2750	2832	2793	2791.667	0.009487	0.790840

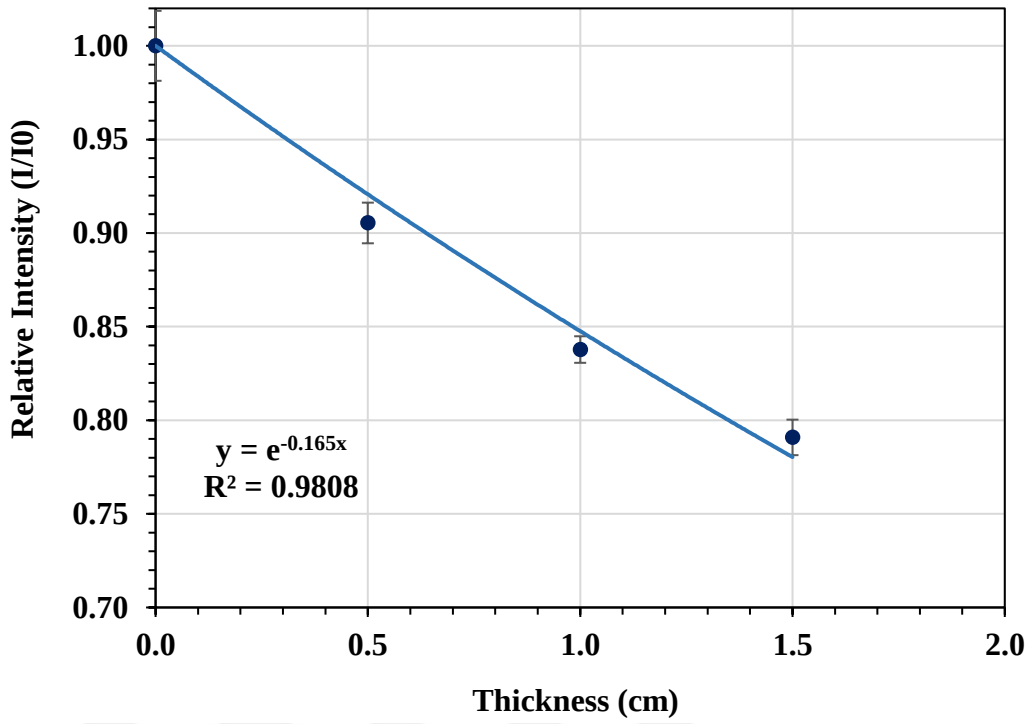

Figure 4.10 : Graph of relative intensity-thickness for PMMA/Colemanite 40 % samples using Co-60 radioisotope (at 1.17 MeV).

Comparison of theoretical and experimental results for Co-60 radioisotope (at 1.17 MeV) was given in Table 4.10. Comparison of gamma attenuation at different colemanite contents for Co-60 radioisotope (at 1.17 MeV) was given in Figure 4.11.

Table 4.10: Comparison of theoretical and experimental results for Co-60 radioisotopes (at 1.17 MeV).

Samples	Linear attenuation coefficients μ (cm^{-1})	Density ρ (g/cm^3)	Mass attenuation coefficients μ/ρ (cm^2/g)	Theoretical mass attenuation coefficients μ/ρ (cm^2/g) (XCOM)	Difference (%)
PMMA	0.106	1.110	0.09549	0.09870	3.2
15 %	0.127	1.216	0.10444	0.11370	8.1
30 %	0.144	1.232	0.11688	0.12110	3.4
40 %	0.165	1.247	0.13231	0.13960	5.2

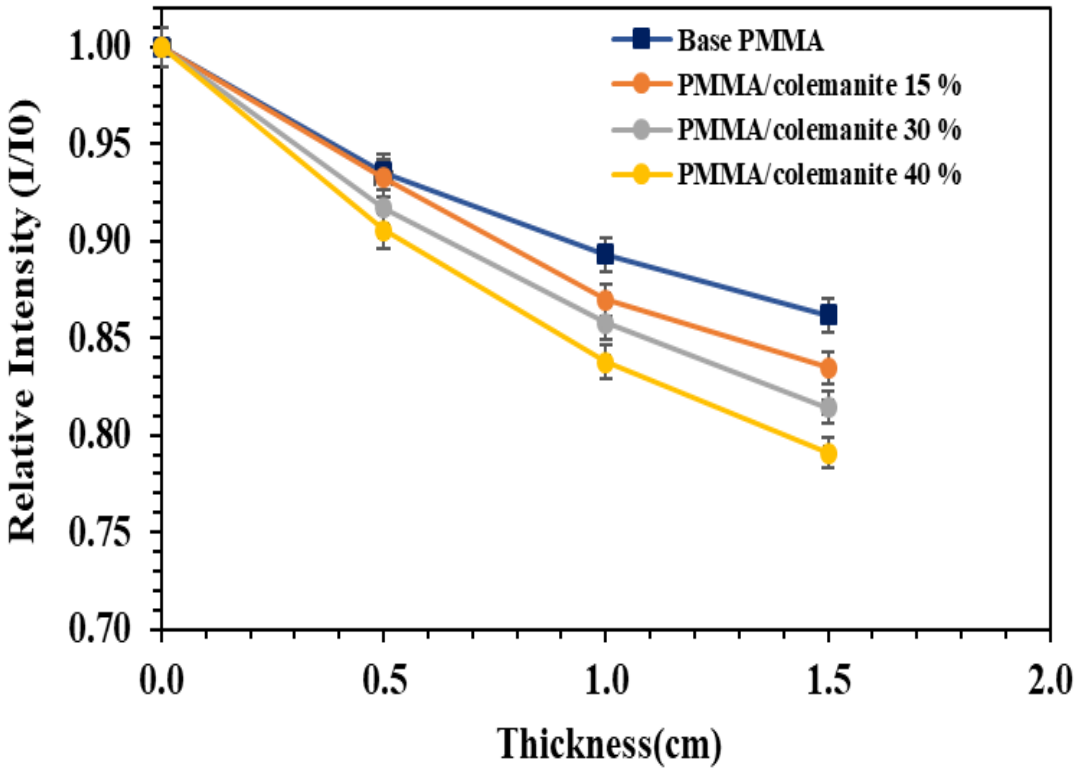

Figure 4.11 : Comparison of gamma radiation attenuation at different colemanite concentrations for Co-60 radioisotope (at 1.17 MeV).

Changes in the relative intensity values of pure PMMA samples were measured by the rise of thickness against Co-60 radioisotope at 1.33 MeV gamma-peak and presented in Table 4.11. The calsulated value for linear attenuation coefficient can be seen in Figure 4.12.

Table 4.11: Results of gamma transmission measurements for pure PMMA using Co-60 radioisotope (at 1.33 MeV).

Thickness (cm)	Count 1	Count 2	Count 3	Average Count	Standard Deviation	Relative Count (I/Io)
0	3853	3735	3848	3812.00	0.01429	1.00000
0.5	3679	3665	3523	3622.33	0.01849	0.95024
1	3470	3338	3433	3413.67	0.01458	0.89551
1.5	3209	3154	3429	3264.00	0.03117	0.85624

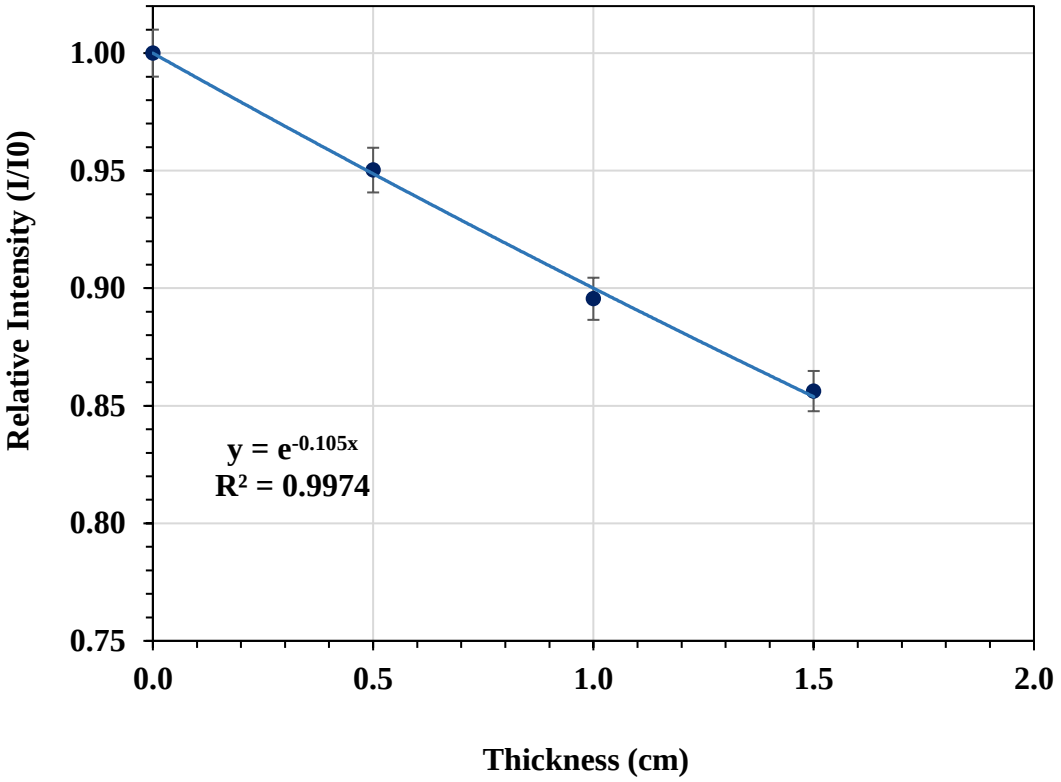

Figure 4.12 : Graph of relative intensity-thickness for pure PMMA using Co-60 radioisotope (at 1.33 MeV).

Results of gamma transmission measurements for PMMA/Colemanite 15 % samples using Co-60 at 1.33 MeV gamma-peak were listed at Table 4.12. Linear attenuation coefficient was given in Figure 4.13.

Table 4.12: Results of gamma transmission measurements for PMMA/Colemanite 15 % samples using Co-60 radioisotope (at 1.33 MeV).

Thickness (cm)	Count 1	Count 2	Count 3	Average Count	Standard Deviation	Relative Count (I/Io)
0	3853	3735	3848	3812.00	0.01429	1.00000
0.5	3515	3597	3521	3544.33	0.00979	0.92978
1	3329	3400	3235	3321.33	0.01773	0.87128
1.5	3190	3194	3227	3203.67	0.00435	0.84042

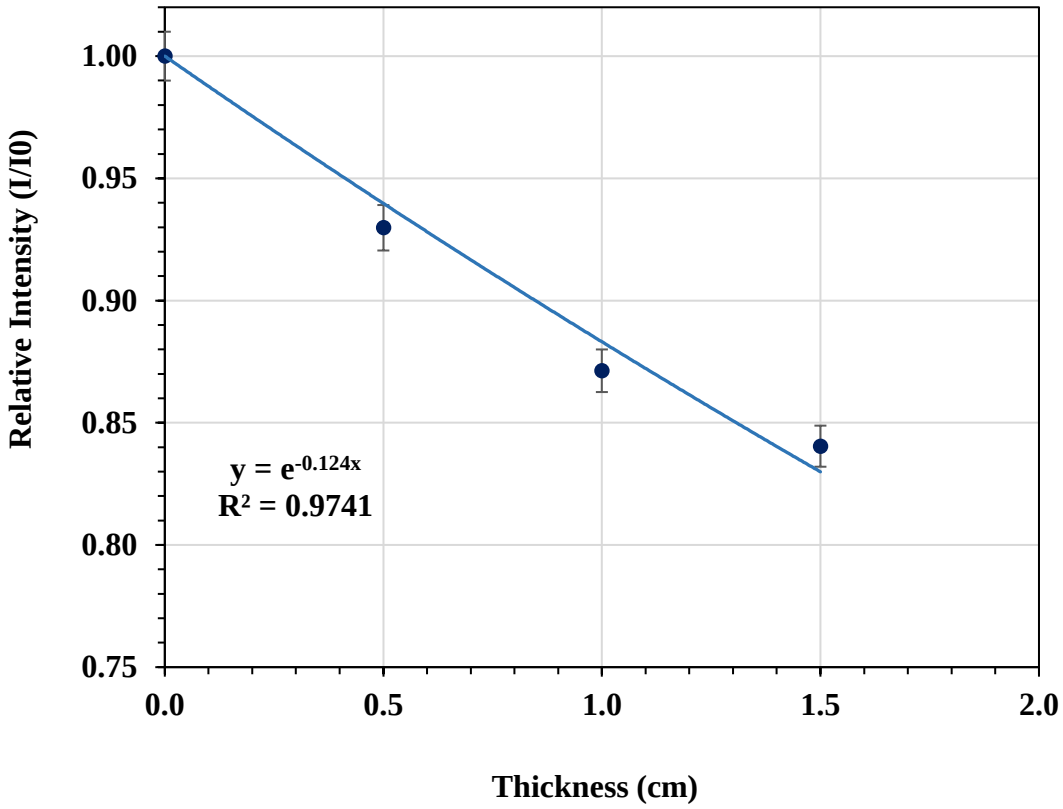

Figure 4.13 : Graph of relative intensity-thickness for PMMA/colemanite 15 % samples using Co-60 radioisotope (at 1.33 MeV).

Result of gamma transmission measurements for PMMA/Colemanite 30 % samples using Co-60 at 1.33 MeV gamma-peak were listed at Table 4.13. Linear attenuation coefficient can be seen in Figure 4.14.

Table 4.13: Results of gamma transmission measurements for PMMA/Colemanite 30 % samples using Co-60 radioisotope (at 1.33 MeV).

Thickness (cm)	Count 1	Count 2	Count 3	Average Count	Standard Deviation	Relative Count (I/Io)
0	3853	3735	3848	3812.00	0.01429	1.00000
0.5	3485	3562	3497	3514.67	0.00887	0.92200
1	3309	3392	3227	3309.33	0.01767	0.86814
1.5	3158	3160	3163	3160.33	0.00054	0.82905

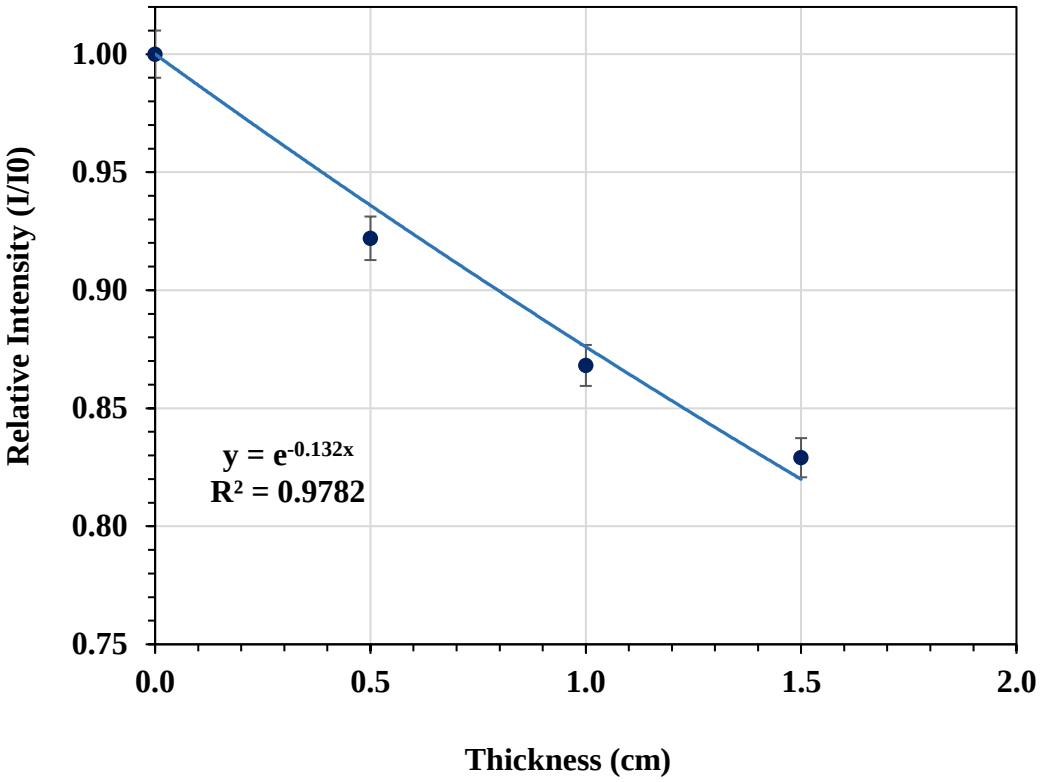

Figure 4.14 : Graph of relative intensity-thickness for PMMA/colemanite 30 % samples using Co-60 radioisotope (at 1.33 MeV).

Results of gamma transmission measurements for PMMA/Colemanite 40 % samples against Co-60 at 1.33 MeV gamma-peak were listed at Table 4.14. The value of linear attenuation coefficient was calculated and presented in the given equation at Figure 4.15.

Table 4.14: Results of gamma transmission measurements for PMMA/Colemanite 40 % samples using Co-60 radioisotope (at 1.33 MeV).

Thickness (cm)	Count 1	Count 2	Count 3	Average Count	Standard Deviation	Relative Count (I/Io)
0	3853	3735	3848	3812.00	0.01429	1.000000
0.5	3466	3583	3468	3505.67	0.01435	0.91964
1	3244	3269	3206	3239.67	0.00679	0.84986
1.5	3087	3084	3065	3078.67	0.00256	0.80763

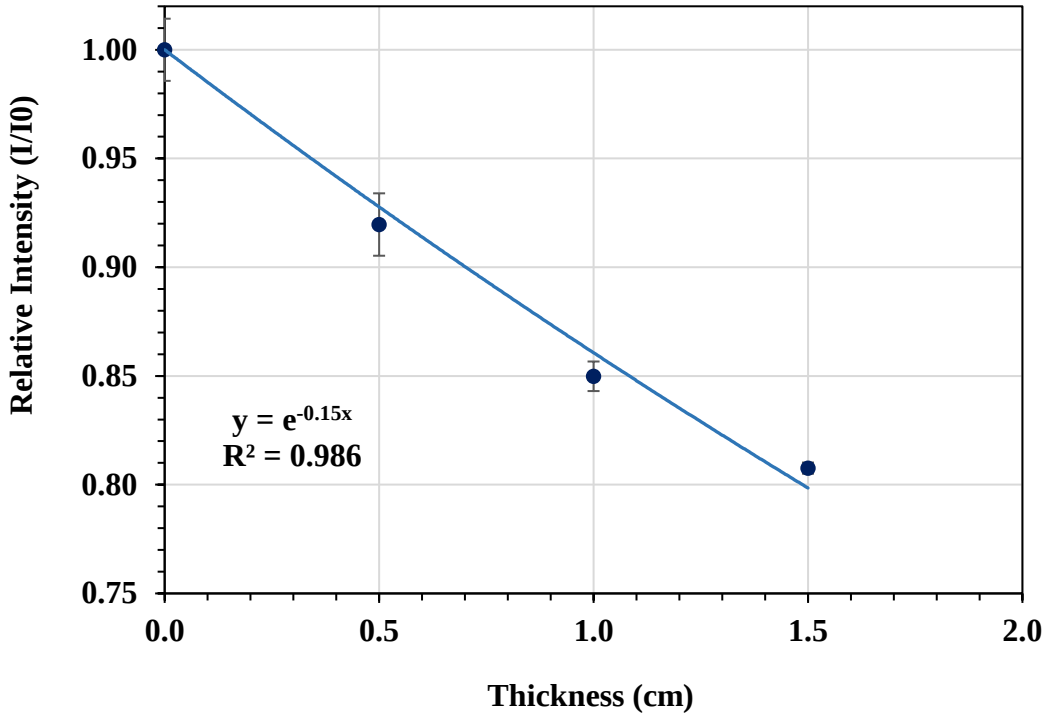

Figure 4.15 : Graph of relative intensity-thickness for PMMA/colemanite 40 % samples using Co-60 radioisotope (at 1.33 MeV).

Comparison theoretical and experimental results for Co-60 radioisotopes (at 1.17 MeV) was given in Table 4.15. Comparison of gamma attenuation at different colemanite contents for Co-60 radioisotope (at 1.33 MeV) was given in Figure 4.16.

Table 4.15: Comparison of theoretical and experimental results for Co-60 radioisotopes (at 1.33 MeV).

Samples	Linear attenuation coefficients μ (cm^{-1})	Density ρ (g/cm^3)	Mass attenuation coefficients μ/ρ (cm^2/g)	Theoretical mass attenuation coefficients μ/ρ (cm^2/g) (XCOM)	Difference (%)
PMMA	0.105	1.110	0.09459	0.09717	2.6
15 %	0.124	1.216	0.10197	0.10200	0.2
30 %	0.132	1.232	0.10714	0.11120	3.6
40 %	0.150	1.247	0.12028	0.12660	4.9

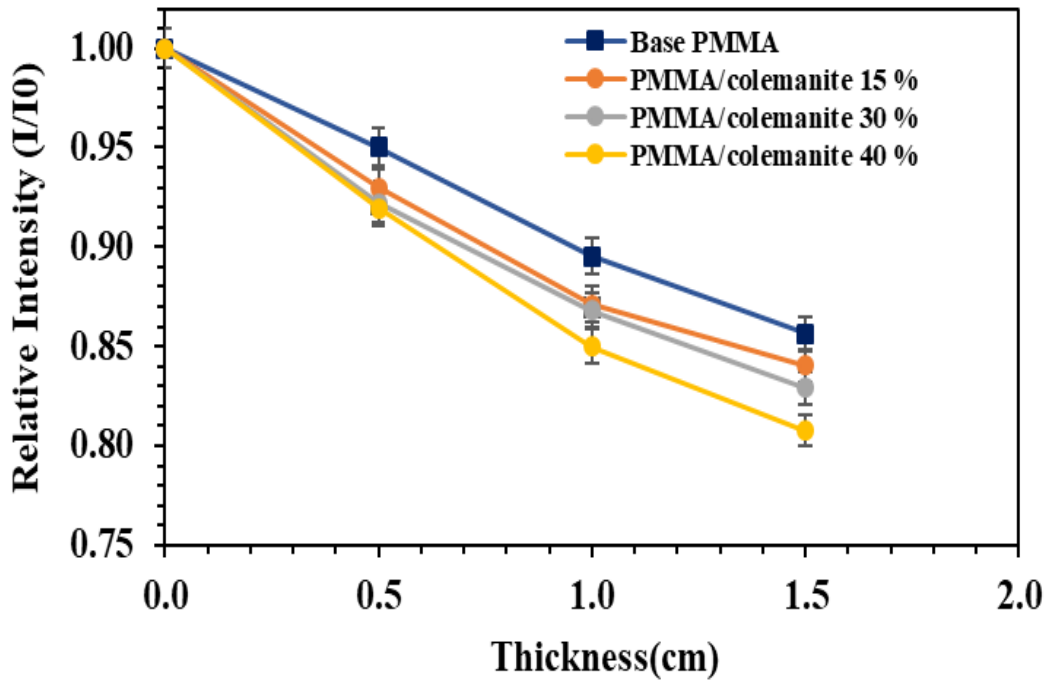

Figure 4.16 : Comparison of gamma radiation attenuation at different colemanite concentrations for Co-60 radioisotope (at 1.33 MeV).

4.2 Neutron Transmission Measurements Using ^{239}Pu-Be Neutron Source

The rise of colemanite concentration in the samples resulted in the variations in relative count (I/Io) against Pu-Be. Total macroscopic cross sections (Σtotal) were obtained from thickness versus relative count graph. Results of pure PMMA for Pu-Be neutron source were listed at Table 4.16. Changes in relative intensity values for pure PMMA samples depending on thickness against neutron source were presented in Figure 4.17.

Table 4.16: Results of neutron transmission measurements for pure PMMA using Pu-Be (neutron source).

Thickness (cm)	Count 1	Count 2	Count 3	Average Count	Standard Deviation	Relative Count (I/Io)
0	1542	3068	4593	3067.667	0.406030	1.0000
0.5	1486	2374	3237	2365.667	0.233033	0.7711
1	1002	2056	2820	1959.333	0.242965	0.6387
1.5	922.0	1752	2786	1820.000	0.248558	0.5932

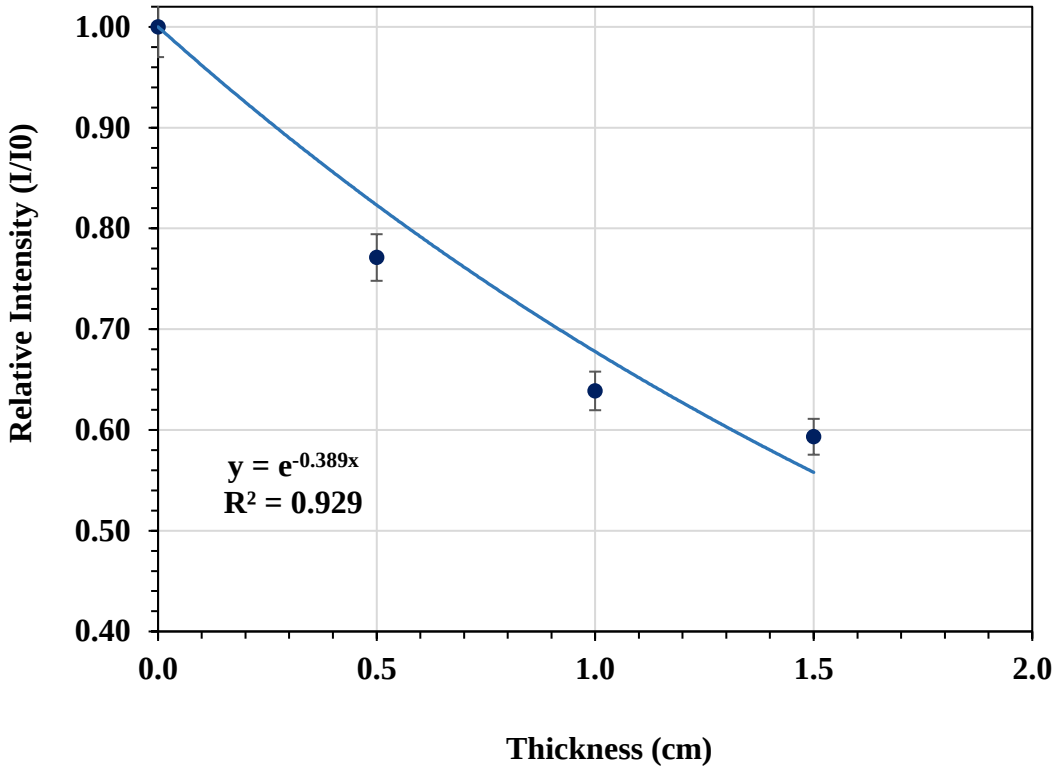

Figure 4.17 : Graph of relative intensity-thickness for pure PMMA using Pu-Be neutron source.

Results of PMMA/Colemanite 15 % samples using Pu-Be as neutron source were listed at Table 4.17. Changes in relative intensity values of PMMA/colemanite composite samples depending on their thicknesses against neutron source were presented in Figure 4.18.

Table 4.17: Results of neutron transmission measurements for PMMA/Colemanite 15 % samples using Pu-Be (neutron source).

Thickness (cm)	Count 1	Count 2	Count 3	Average Count	Standard Deviation	Relative Count (I/Io)
0	1542	3068	4593	3067.667	0.406030	1.0000
0.5	1430	2278	3185	2297.667	0.233601	0.7487
1	920.0	1923	2773	1872.000	0.246879	0.6102
1.5	910.0	1634	2605	1716.333	0.226369	0.5594

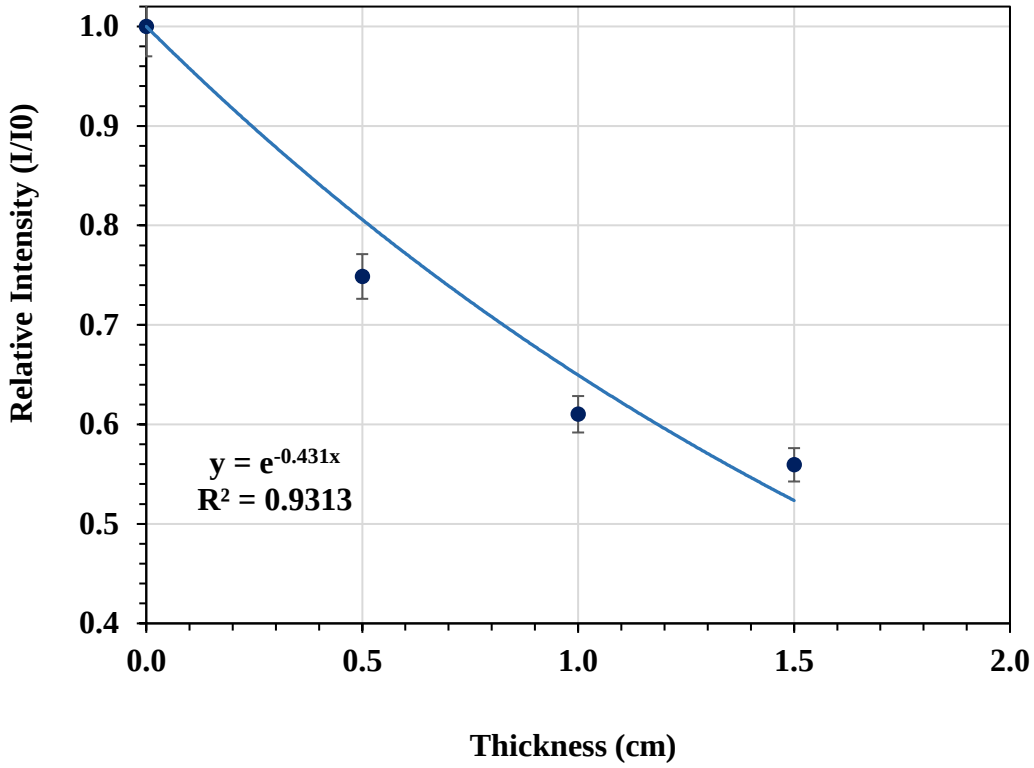

Figure 4.18 : Graph of relative intensity-thickness for PMMA/Colemanite 15 % samples using Pu-Be neutron source.

Results of PMMA/Colemanite 30 % samples using Pu-Be as neutron source were listed at Table 4.18. Changes in relative intensity values of the prepared samples depending on their thicknesses against neutron source were measured and presented in Figure 4.19.

Table 4.18: Results of neutron transmission measurements for PMMA/Colemanite 30 % samples using Pu-Be (neutron source).

Thickness (cm)	Count 1	Count 2	Count 3	Average Count	Standard Deviation	Relative Count (I/Io)
0	1542	3068	4593	3067.667	0.406030	1.0000
0.5	1356	2143	3086	2195.000	0.230542	0.7155
1	900.0	1832	2699	1810.333	0.239465	0.5901
1.5	881.0	1719	2332	1644.000	0.193873	0.5359

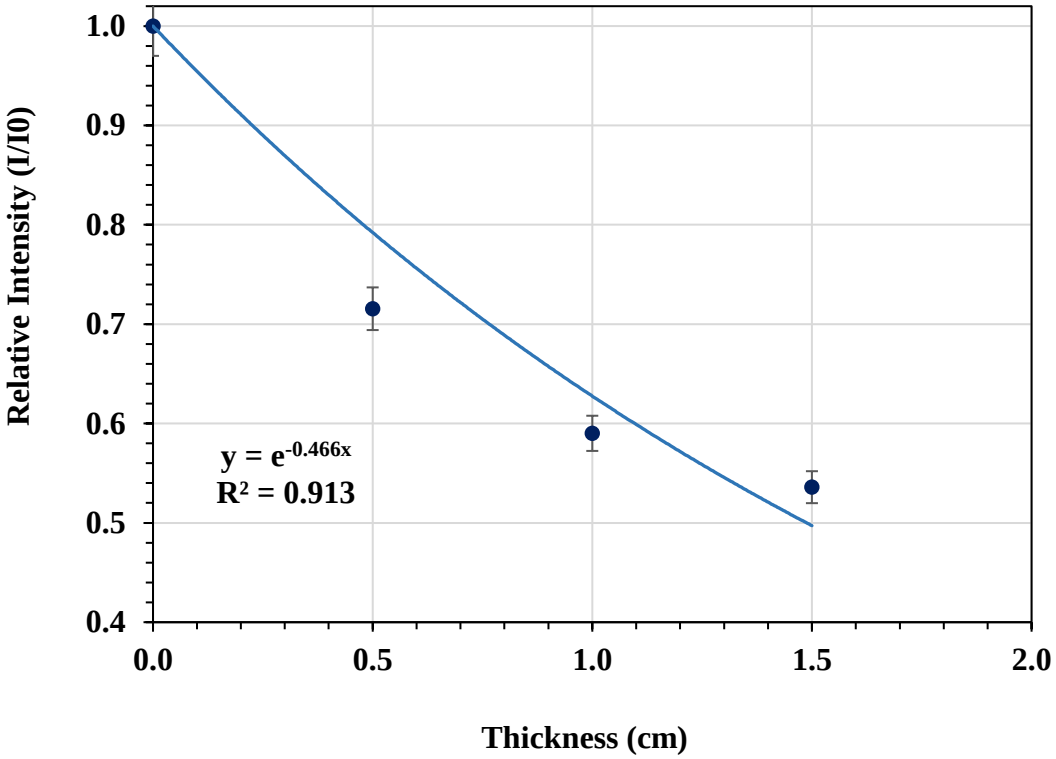

Figure 4.19 : Graph of relative intensity-thickness for PMMA/Colemanite 30 % samples using Pu-Be neutron source.

Results of PMMA/Colemanite 40 % samples using Pu-Be as neutron source were listed at Table 4.19. Changes in the relative intensity values of examined samples depending on their thicknesses against neutron source were measured and shown in Figure 4.20.

Table 4.19: Results of neutron transmission measurements for PMMA/Colemanite 40 % samples using Pu-Be (neutron source).

Thickness (cm)	Count 1	Count 2	Count 3	Average Count	Standard Deviation	Relative Count (I/Io)
0	1542	3068	4593	3067.667	0.406030	1.0000
0.5	1294	1988	2780	2020.667	0.197902	0.6586
1	947.0	1456	2205	1536.000	0.168428	0.5007
1.5	686.0	1292	2080	1352.667	0.186041	0.4409

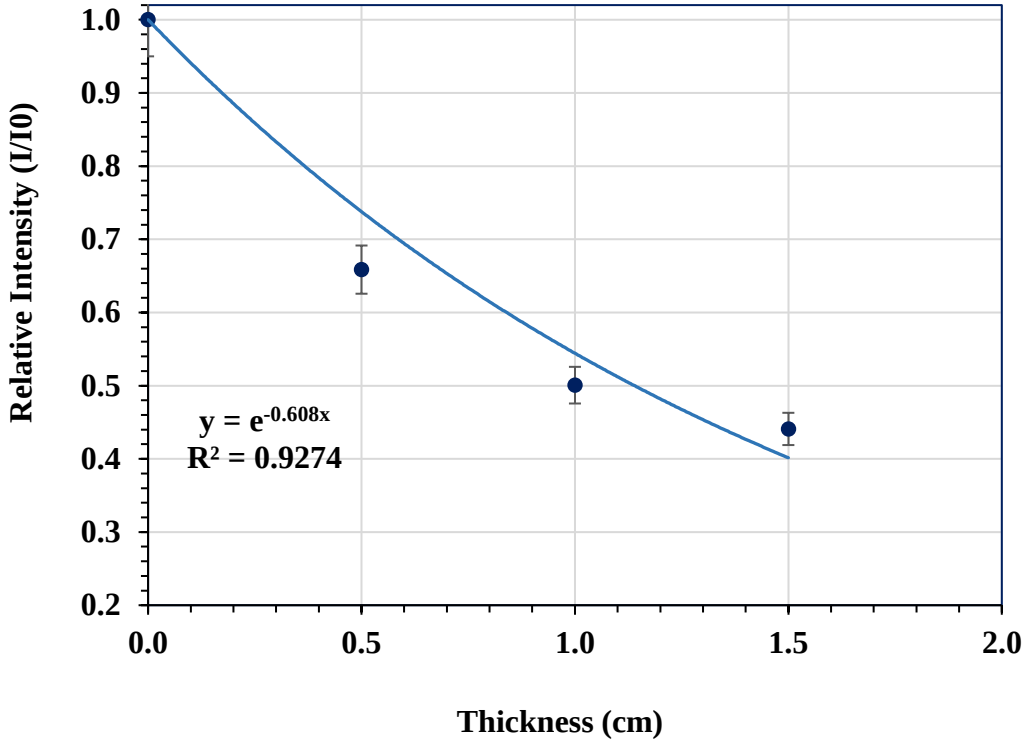

Figure 4.20 : Graph of relative intensity-thickness for PMMA/Colemanite 40 % samples using Pu-Be neutron source.

Total macroscopic cross sections (Σ_T) for PMMA/Colemanite composite samples were obtained from relative intensity curve using Equation 2.4. The calculated total macroscopic cross sections for samples using Pu-Be as neutron source were used to determine the neutron attenuation at composite with rise of colemanite concentration. Total macroscopic cross sections for PMMA/Colemanite composite samples were given in Table 4.20. Comparison of neutron attenuation at different colemanite concentrations for Pu-Be neutron source was given in Figure 4.21.

Table 4.20: Results of total macroscopic cross-sections for PMMA/Colemanite composite samples using Pu-Be (neutron source).

Samples	The total macroscopic cross-sections (Σ_T) (cm^{-1})	Mean free path $1/\Sigma_T$ (cm)
PMMA	0.389	2.570
15 %	0.431	2.320
30 %	0.466	2.145
40 %	0.608	1.644

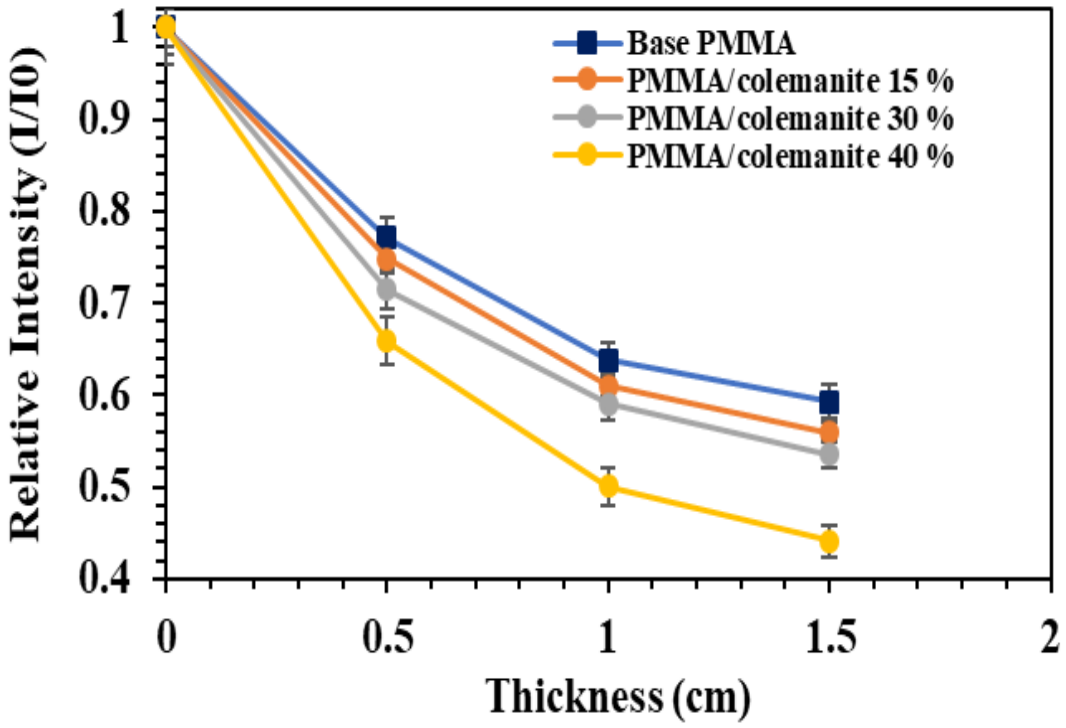

Figure 4.21 : Comparison of neutron attenuation at different colemanite concentrations for Pu-Be neutron source.

4.3 Beta Transmission Measurements Using Sr-90 Radioisotope

Results of pure PMMA samples using Sr-90 were given in Table 4.21. The changes of relative intensity values for pure PMMA samples with rise of thickness were given in Figure 4.22.

Table 4.21: Results of beta transmission measurements for pure PMMA samples using Sr-90 (beta source).

Thickness (cm)	Count 1	Count 2	Count 3	Average Count	Standard Deviation	Relative Count (I/Io)
0	0.13	0.13	0.12	0.126667	0.004714	1.0000
0.5	0.11	0.12	0.11	0.113333	0.004714	0.8947
1	0.10	0.11	0.10	0.103333	0.005774	0.8157
1.5	0.10	0.09	0.10	0.096667	0.004714	0.7631

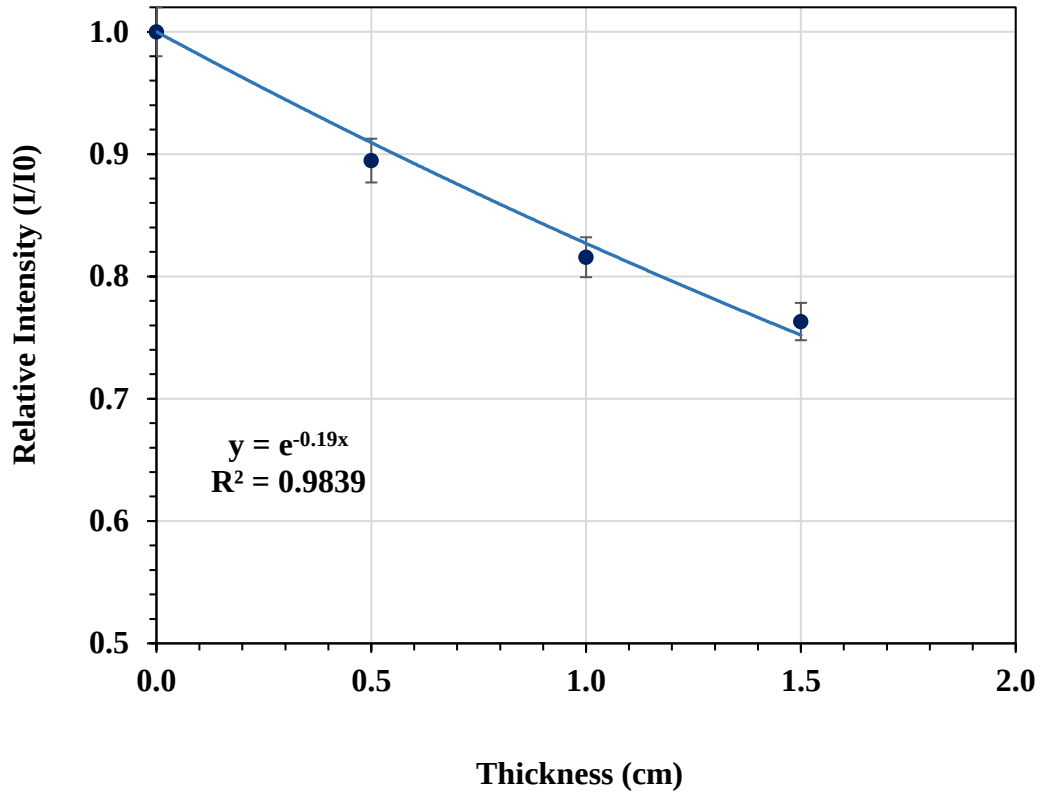

Figure 4.22 : Graph of relative intensity-thickness for pure PMMA using Sr-90 radioisotope.

Results of the PMMA/colemanite 15 % samples against Sr-90 radioisotope were listed at Table 4.22. Changes of relative intensity values for samples with the rise of thickness were presented in Figure 4.23.

Table 4.22: Results of beta transmission measurements for PMMA/Colemanite 15 % samples using Sr-90 (beta source).

Thickness (cm)	Count 1	Count 2	Count 3	Average Count	Standard Deviation	Relative Count (I/Io)
0	0.13	0.13	0.12	0.12667	0.00577	1.0000
0.5	0.11	0.10	0.10	0.10333	0.00577	0.8157
1	0.09	0.08	0.09	0.08667	0.00577	0.6842
1.5	0.07	0.08	0.08	0.07667	0.00577	0.6052

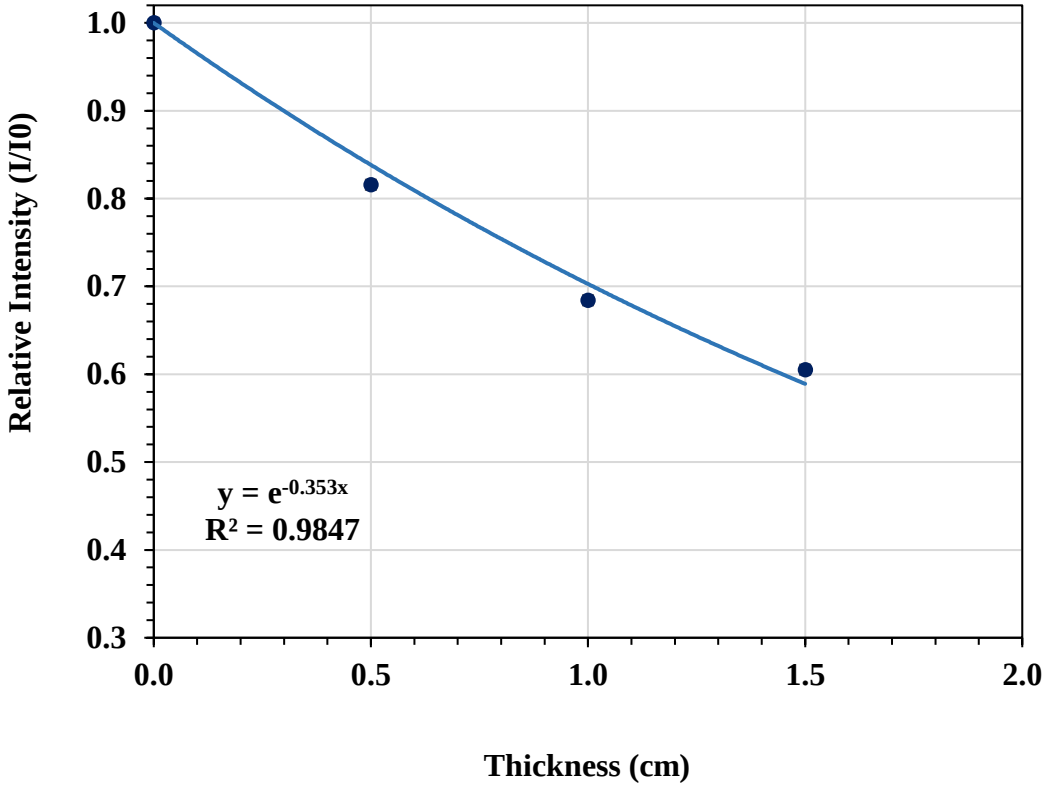

Figure 4.23 : Graph of relative intensity-thickness for PMMA/Colemanite 15 % using Sr-90 radioisotope.

Results of the PMMA/colemanite 30 % samples against Sr-90 radioisotope were listed at Table 4.23. Changes in relative intensity values of samples with the rise of thickness were shown in Figure 4.24.

Table 4.23: Results of beta transmission measurements for PMMA/Colemanite 30 % samples using Sr-90 (beta source).

Thickness (cm)	Count 1	Count 2	Count 3	Average Count	Standard Deviation	Relative Count (I/Io)
0	0.13	0.13	0.12	0.12667	0.00471	1.0000
0.5	0.10	0.09	0.10	0.09667	0.00471	0.7631
1	0.08	0.07	0.08	0.07667	0.00471	0.6052
1.5	0.08	0.06	0.07	0.07000	0.00816	0.5526

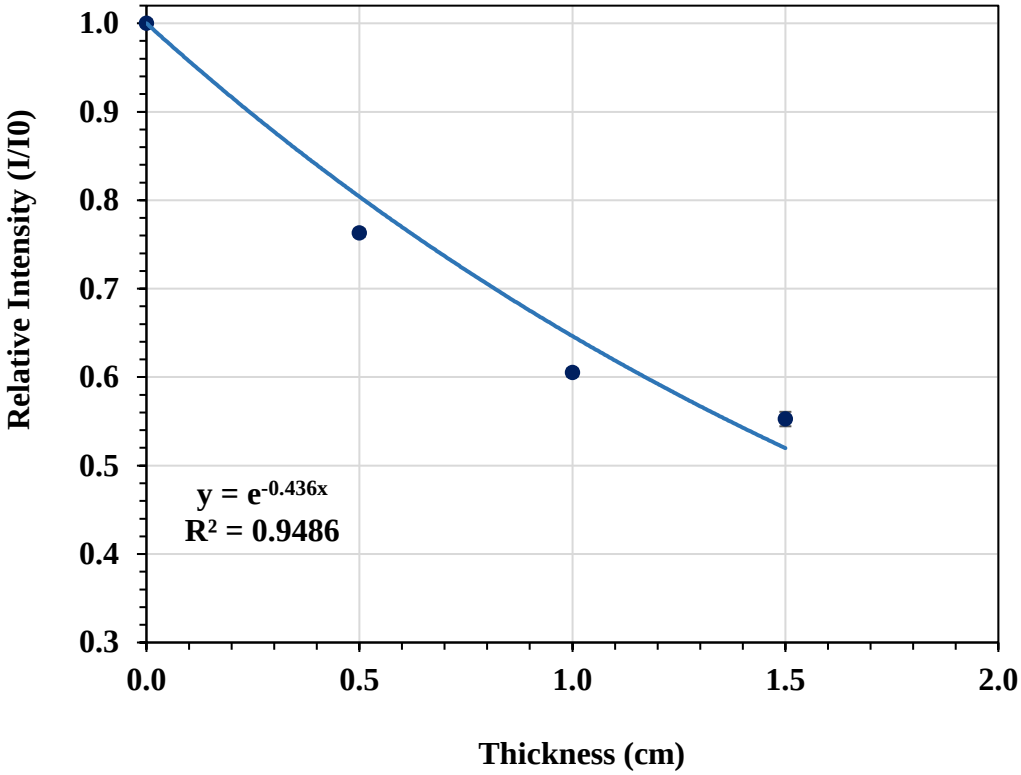

Figure 4.24 : Graph of relative intensity-thickness for PMMA/Colemanite 30 % using Sr-90 radioisotope.

Results for the PMMA/colemanite 40 % samples against Sr-90 radioisotope were listed in Table 4.24. Changes in the relative intensity values of PMMA/colemanite composite samples with the rise of thickness were measured and illustrated in Figure 4.25.

Table 4.24: Results of beta transmission measurements for PMMA/Colemanite 40 % samples using Sr-90 (beta source).

Thickness (cm)	Count 1	Count 2	Count 3	Average Count	Standard Deviation	Relative Count (I/Io)
0	0.13	0.13	0.12	0.12667	0.00471	1.0000
0.5	0.08	0.08	0.09	0.08333	0.00471	0.6578
1	0.06	0.07	0.07	0.06667	0.00471	0.5263
1.5	0.06	0.05	0.06	0.05667	0.00471	0.4473

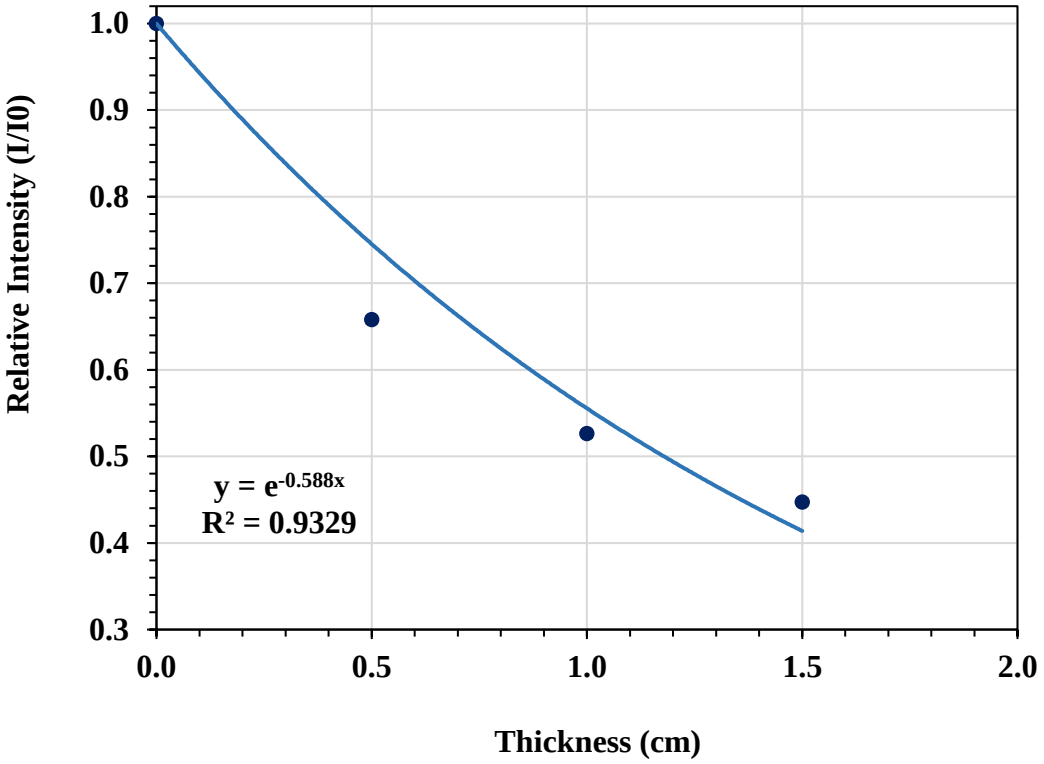

Figure 4.25 : Graph of relative intensity-thickness for PMMA/Colemanite 40 % using Sr-90 radioisotope.

The experimental results of linear and mass attenuation for Sr-90 radioisotopes were listed at Table 4.25. Comparison of beta attenuation at different colemanite concentrations for Sr-90 radioisotope was given in Figure 4.26.

Table 4.25: Results for linear and mass attenuation coefficients using Sr-90 radioisotopes.

Samples	Linear attenuation coefficients μ (cm^{-1})	Density ρ (g/cm^3)	Mass attenuation coefficients μ/ρ (cm^2/g)
PMMA	0.190	1.110	0.17117
15 %	0.353	1.216	0.29029
30 %	0.436	1.232	0.35389
40 %	0.588	1.247	0.47153

The effect of irradiation on radiation attenuation properties can be explained by the obtained linear and mass attenuation coefficients for PMMA/Colemanite composite samples.

The results of this experiment enabled us to compare the linear attenuation coefficient values for gamma and beta sources together with the obtained values of total macroscopic cross sections for neutron source.

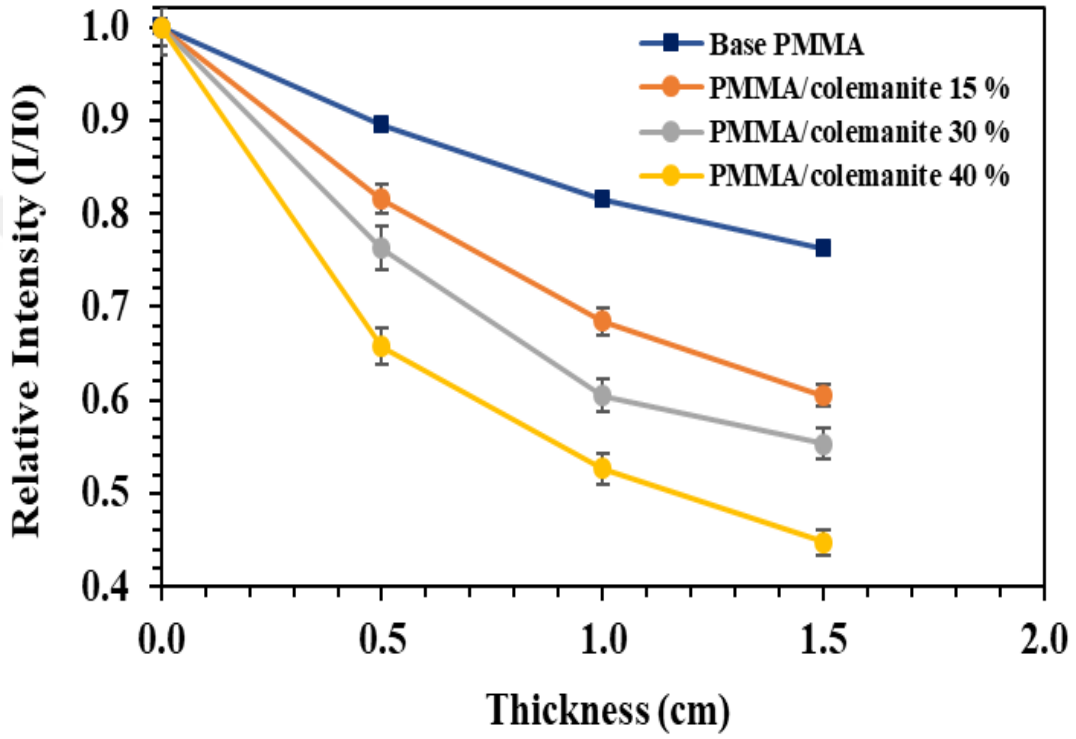

Figure 4.26 : Comparison of beta attenuation at different colemanite concentrations for Sr-90 radioisotope.

Half-value layer (HVL) is defined as a thickness that is required to stop half of the coming radiation. The half-value thicknesses of PMMA/Colemanite composite samples were determined from experimental values for linear attenuation coefficients (μ) using Cs-137, Co-60 and Sr-90 radioisotopes and total macroscopic cross-sections (Σ_T) for neutrons in equations below:

$$HVL = ln2/\mu = 0.693/\mu \quad (4.1)$$

$$HVL = ln2/\Sigma_T = 0.693/\Sigma_T \quad (4.2)$$

The results of the Half-value layer for pure PMMA and PMMA/Colemanite composite samples using Cs- 137, Co-60 as gamma sources were listed in Table 4.26.

The obtained results for half value layer thicknesses of the examined samples were compared based on gamma energies at different colemanite concentrations in Figure 4.27.

Table 4.26: HVL values for PMMA and PMMA/Colemanite composite samples using Cs- 137 and Co-60 (gamma sources).

Samples	HVL (cm) for Cs-137 radioisotope	HVL (cm) for Co-60 radioisotope (at 1.17 MeV)	HVL (cm) for Co-60 radioisotope (at 1.33 MeV)
PMMA	6.187	6.537	6.600
15 %	5.171	5.456	5.588
30 %	4.076	4.812	5.250
40 %	3.666	4.200	4.620

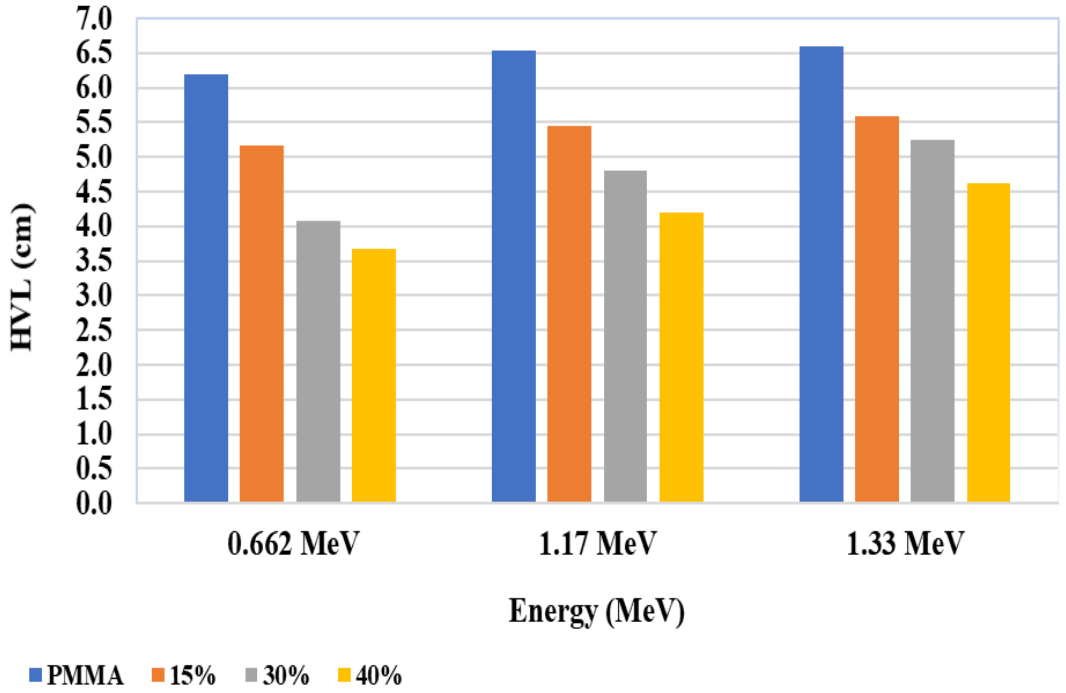

Figure 4.27 : Comparison of HVL thicknesses at different gamma energies.

Results of the HVL values for PMMA/Colemanite composite samples against Pu–Be (NH3) and Sr-90 radioisotope were calculated in Table 4.27.

The obtained results for HVL thicknesses of samples were compared based on colemanite concentrations for neutron particles in Figure 4.28.

Table 4.27: HVL values for PMMA and PMMA/Colemanite composite samples using Pu–Be (NH3) and Sr-90 radioisotope.

Samples	HVL (cm) for Pu-Be (NH3)	HVL (cm) for Sr-90 radioisotope
PMMA	1.781	3.647
15 %	1.607	1.963
30 %	1.487	1.589
40 %	1.139	1.178

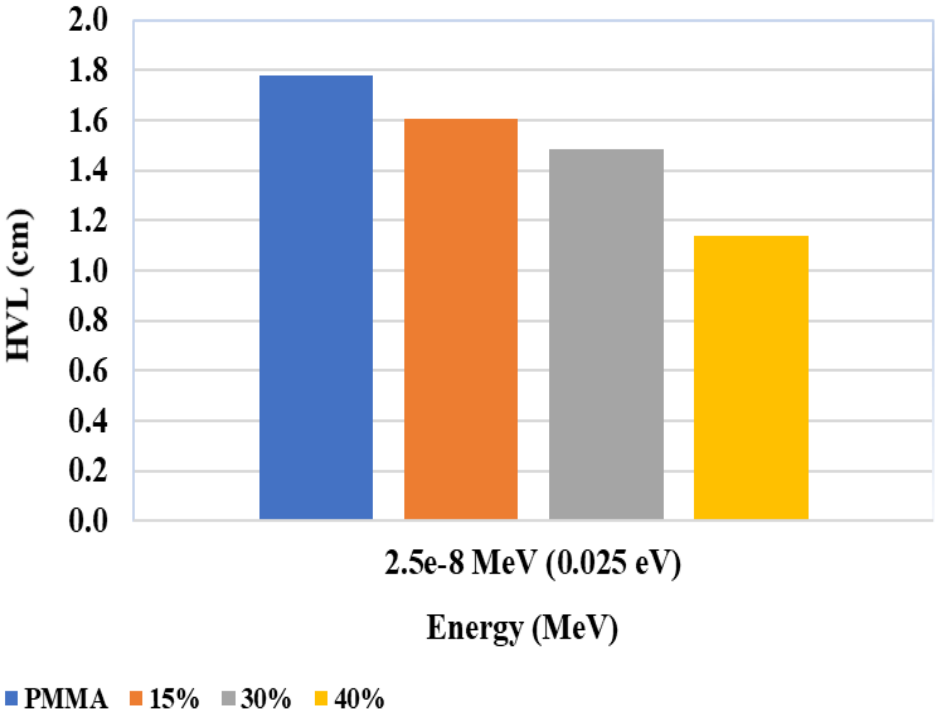

Figure 4.28 : Comparison of HVL thicknesses for neutron particles at different colemanite concentrations.

The obtained results for HVL thicknesses of samples were compared based on colemanite concentrations for beta particles in Figure 4.29.

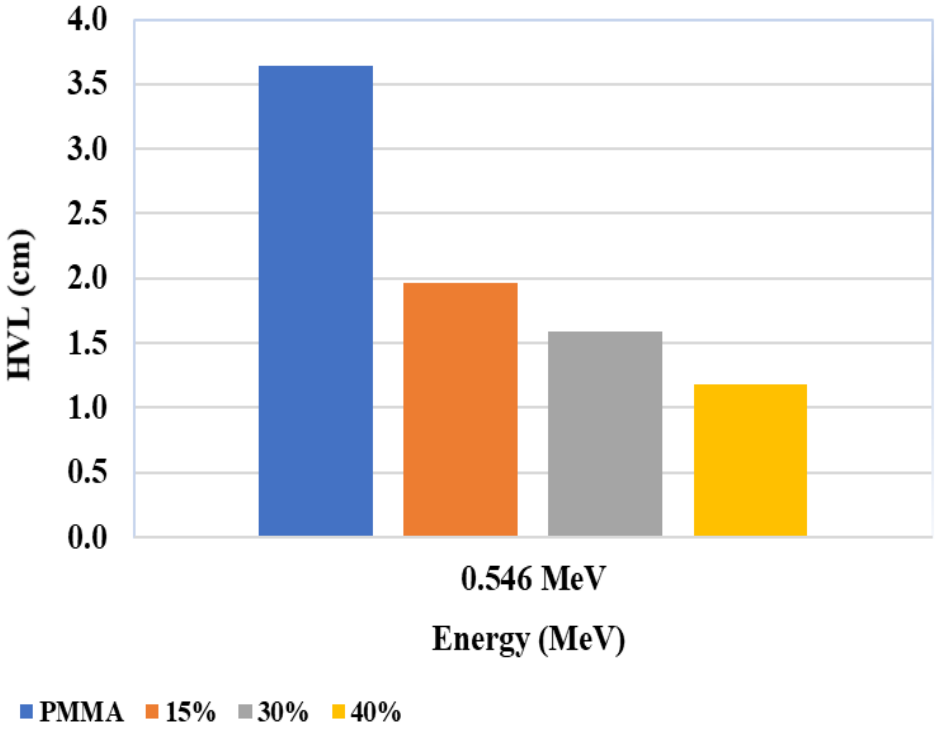

Figure 4.29 : Comparison of HVL thicknesses for beta particles at different colemanite concentrations.

5. CONCLUSION

This study was performed in order to understand the influence of colemanite filler on Poly (methyl methacrylate) polymer matrices and the corresponding improvements in the radiation attenuation properties of PMMA base Polymer/colemanite composites against beta, neutron and gamma sources for shielding purposes.

ATRP technique was used to produce PMMA. Then, the colemanite filler was dispersed in the produced PMMA by in situ polymerization method. This method was an effective method to obtain homogeneous dispersion in PMMA/Colemanite composite samples.

The beta, neutron and gamma transmission techniques were utilized to study radiation shielding performance for PMMA/Colemanite composite samples at different colemanite concentrations against beta, gamma and neutron sources. Linear attenuation coefficient for PMMA/Colemanite composite samples improved slightly by the rise of the colemanite filler amount in the PMMA polymer. Then, the obtained experimental attenuation coefficient from the experiment were compared with theoretical attenuation coefficient calculated in XCOM program. The result of this comparison determined that there was a similarity between obtained theoretical and experimental attenuation coefficients. Using Pu-Be Neutron Howitzer, the effect of added colemanite in the PMMA/Colemanite composite samples was examined. The results indicated that there was a rise in the total macroscopic cross-sections values with the addition of colemanite filler into the PMMA polymer.

HVL values for all of the samples against beta, neutron and gamma radiation from the used four sources was calculated. In order to the obtained results, the HVL values were reduced by the increase of the colemanite concentration in PMMA/Colemanite samples. HVL is the required thickness of the samples that attenuates the half of the incident ionizing radiation. Thus, the addition of colemanite to the PMMA polymer improved its attenuation properties.

The PMMA reinforced by different fillers such as colemanite can be examined to perform at various lightweight material applications. In this study, the obtained results indicated that PMMA/Colemanite composites produced by ATRP method can be used as a suitable material in several application areas such as the aviation and aerospace industries.

REFERENCES

[1] Cowie, J. M. G. (1991). "Polymers: Chemistry and Physics of Modern Materials*",* *2nd Edition,* Taylor & Francis.

[2] Young, R. J., Lovell, P. A. (2011). "Introduction to Polymers*", Third Edition,* Taylor & Francis.

[3] Webster, O. W. (1990). **"**Living Polymerization Methods*"*,Central Research and Development, Du Pont, P.O. Box 80328, Wilmington, DE 19880-0328.

[4] Helmenstine, A. M. (2019). "Monomers and Polymers in Chemistry". thoughtco.com/monomers-and-polymers-intro-608928.

[5] Lampman, S. (2003). "Characterization and Failure Analysis of Plastics*",* ASM International.

[6] Ebewele, R. O. (2000). "Polymer Science and Technology*",* CRC Press.

[7] Maheri, M.R., Adams, R.D., Gaitonde, J.M. (1996). " The effect of temperature on the dynamic characteristics of heat-resistant thermoplastic composites". Composites Science and Technology.

[8] Muzzy, J. D., Kays, A. O. (1984)."Thermoplastic vs. thermosetting structural composites*"*. https://doi.org/10.1002/pc.750050302.

[9] Harper, C. A., Petrie, E. M. (2003). "Plastics Materials and Processes: A Concise Encyclopedia*"*, Wiley.

[10] Ellis, B., Smith, R. (2008). "Polymers: A Property Database*", Second Edition,* CRC Press.

[11] Biron, M. (2007). "Thermoplastics and Thermoplastic Composites: Technical Information for Plastics Users*"*, Elsevier Science.

[12] Olabisi, O., Adewale, K. (2016). "Handbook of Thermoplastics*", Second Edition,* CRC Press.

[13] Simon, J. M., Smith, R. A. (2000) "Borate raw materials*"*. Volume 41, Number 6 pp. 169-173(5) Society of Glass Technology, USA.

[14] Frost, R. L., Scholz, R., Ruan, X., Fernandes Lima, R. M. (2016). "Thermal analysis and infrared emission spectroscopy of the borate mineral colemanite ($CaB_3O_4(OH)_3 \cdot H_2O$)*"*. Journal of Thermal Analysis and Calorimetry.

[15] Sahin, T. (2011). "Mechanical and Thermal Properties of Colemanite Filled Polypropylene*"*.

[16] Tanrikulu, Y. E., Yaşar, A. (2017). "Investigation of Mechanical and Thermal Properties of Boron Minerals Doped Plastic Materials*"*. Çukurova University Journal of the Faculty of Engineering and Architecture.

[17] Colebrooke, H. T., Colenso, J. W. "1911 Encyclopædia Britannica*"*. *eleventh edition.*

[18] Özdemir, O., Çelik, M. S. (2010). "Surface Properties and Flotation Characteristics of Boron Minerals*"*. The Open Mineral Processing Journal.

[19] Yazici, Z. O., Helvaci, A., Akpınar, S. (2016). "Microwave Assisted Calcination of Colemanite Powders*"*. doi: 10.15344/2455-2372/2016/129.

[20] Celik, A. G., Cakal, G. O. (2014). "Characterization of Espey Colemanite and Variation of Its Physical Properties with Temperature*"*. Physicochemical Problems of Mineral Processing.

[21] Eymir, Ç., Okur, H. (2005) Dehydration of ulexite by microwave heating. Thermochimica Acta 428: 125-129.

[22] Waclawska, I., Stoch, L., Paulik, J., Paulik, F. (1988) Thermal Decomposition of Colemanite. Thermochimica Acta 126: 307-318.

[23] Ediz, N., Yurdakul, H. (2009) Development of body formulations using colemanite waste in porcelain tile production. Journal of Ceramic Processing Research 10: 758-769.

[24] Winey, K. I., Vaia, R. A. (2007). "Polymer nanocomposites*"*, MRS bulletin, 32, 314-322. Cambridge University Press.

[25] Khan, W. S., Hamadneh, N. N., Khan, W. A. (2016). **"**Polymer nanocomposites– synthesis techniques, classification and properties*"*. One Central Press (OCP).

[26] Xia, J., Matyjaszewski, K. (1997). Controlled/"Living" Radical Polymerization. Atom Transfer Radical Polymerization Using Multidentate Amine Ligands, *Macromolecules*, 30, 7697-7700.

[27] Matyjaszewski, K., Xia, J. (2001). "Atom transfer radical polymerization", *Chemical reviews*, 101, 2921-2990.

[28] Matyjaszewski, K., Davis, T. P. (2003). "Handbook of Radical Polymerization", Wiley.

[29] Tian, B. Y., Hu, P. J., Yuan, M., Tang, E. J., Liu, S. J., Zhao, X. Y., Zhao, D. S. (2012). **"**Effect of different ligands on the controlled polymerization of monodisperse polystyrene nanospheres by atom transfer radical polymerization in an aqueous emulsion"

[30] Li, B., Zhong, W.-H. (2011). "Review on polymer/graphite nanoplatelet nanocomposites*"*, Journal of Materials Science, 46, 5595-5614.

[31] Potts, J. R., Dreyer, D. R., Bielawski, C. W., Ruoff, R. S. (2011). "Graphenebased polymer nanocomposites", Polymer, 52, 5-25.

[32] Aliofkhazraei, M., Ali, N., Milne, W. I., Ozkan, C. S., Mitura, S., Gervasoni, J. L. (2016). "Graphene Science Handbook: Electrical and Optical Properties*"*, CRC Press.

[33] Sengupta, R., Bhattacharya, M., Bandyopadhyay, S., Bhowmick, A. K. (2011). "A review on the mechanical and electrical properties of graphite and modified graphite reinforced polymer composites*"*, Progress in polymer science, 36, 638-670.

[34] Stabin, M. G. (2007). "Radiation Protection and Dosimetry: An Introduction to Health Physics*"*, Springer New York.

[35] Nelson, G., Reilly, D. (1991). "Gamma-ray interactions with matter, Passive Nondestructive Analysis of Nuclear Materials*"*, Los Alamos National Laboratory, *NUREG/CR-5550, LAUR-90-732*, 27-42.

[36] Clegg, D. W., Collyer, A. A. (1991). "Irradiation Effects on Polymers*"*, Springer Netherlands.

[37] Sarray, E. H. A.; Jabbar, A. S. (2018). "Investigate the Ability of the Eggshell to Attenuate the Gamma and Beta Rays as Compared with Composite FeSO4.7H2O*"*. Nucl. Sci. 2018, 3, 16–22. doi: 10.11648/j.ns.20180301.13.

[38] Matur, U. C., Baydogan, N. (2017). "Changes in gamma attenuation behaviour of sol-gel derived CIGS thin film irradiated using Co-60 radioisotope*"*, Journal of Alloys and Compounds, 695, 1405-1413.

[39] Adlien_e, D. (2017). "Basic Radiation Physics and Sources of Radiation. In Applications of _Ionizing Radiation in Materials Processing"; Sun, Y., Chmielewski, A. G., Eds.; Institute of Nuclear Chemistry and Technology: Warszawa, 2017; p. 7.

[40] Baydogan, N.; Ozdemir, O.; Cimenoglu, H. (2013). "The _Improvement in the Electrical Properties of Nanospherical ZnO:Al Thin Film EXPOSED to irradiation Using a Co-60 Radioisotope". Radiat. Phys. Chem. 2013, 89, 20–27. doi:10.1016/j.radphyschem. 2013.02.042.

[41] Kaniappan, K.; Latha, S. (2011), *"*Certain Investigations on the Formulation and Characterization of Polystyrene / Poly(methyl methacrylate) Blends*"*. Department of Chemistry, PSG College of Technology, Coimbatore-641 004, Tamil Nadu, India.

[42] Serway, Raymond A. (1990). *"*Physics for Scientists and Engineers with Modern Physics*", 3rd Ed*., Saunders College.

[43] Rohlf, J. W. (1994). *"*Modern Physics from a to Z0*",* Wiley.

[44] Ulağ, S. (2017). *The Investigation of The Irradiation Effect on PMMA/MWCNTs Polymer Nanocomposites*, (Master's thesis), Retrieved from https://polen.itu.edu.tr/handle/11527/15778

CURRICULUM VITAE

Name Surname: Shima MEHRANPOUR

E-Mail: mehranpour17@itu.edu.tr

EDUCATION: Master of Radiation Science and Technology

B.Sc.: 2014, Urmia University, Faculty of Science, Nuclear Physics